OCEANOLOGIA

ORIGINAL RESEARCH ARTICLE

Element enrichment and provenance of the detrital component in Holocene sediments from the western Black Sea

Vesselin M. Dekov[a,b,*], Valentina Y. Darakchieva[c], Kjell Billström[d],
C. Dieter Garbe-Schönberg[e], George D. Kamenov[f], Morgane Gallinari[g],
Lyubomir Dimitrov[h], Olivier Ragueneau[g], Ellen Kooijman[d]

[a] Tokyo University of Marine Science and Technology, Konan, Minato-ku, Tokyo, Japan
[b] Department of Marine Geosciences, IFREMER, Plouzané, France
[c] Institute of Mineralogy and Crystallography, Bulgarian Academy of Sciences, Sofia, Bulgaria
[d] Department of Geosciences, Swedish Museum of Natural History, Stockholm, Sweden
[e] Institute of Geosciences, Marine Climate Research, University of Kiel, Kiel, Germany
[f] Department of Geological Sciences, University of Florida, Gainesville, FL, USA
[g] UMR CNRS/UBO 6539 LEMAR, European Institute for Marine Studies, Technopôle Brest-Iroise, Plouzané, France
[h] Institute of Oceanology, Bulgarian Academy of Sciences, Varna, Bulgaria

Summary   Concentrations of a large set of major and trace elements, and Sr, Nd and Pb isotope ratios were measured in Holocene sediments cored in the western deep Black Sea in order to unravel: (1) the controls of element enrichment, and (2) sources of the detrital component. The transition of the basin from oxic to euxinic resulted in enrichment or depletion in a number of elements in the deep-sea sediments. Authigenic Fe enrichment appears to depend on the amount of Fe mobilized from the sediment through the benthic redox shuttle mechanism and free H_2S in the water column (degree of "euxinization"). Manganese enrichment is controlled by diagenetic reactions within the sediment: the dissolution of Mn minerals, Mn^{2+} diffusion upward and reprecipitation. Barium enrichment is also controlled by diagenetic reactions, sulfate

 * Corresponding author at: Tokyo University of Marine Science and Technology, 4-5-7 Konan, Minato-ku, Tokyo 108-8477, Japan; Department of Marine Geosciences, IFREMER, 29280 Plouzané, France; Tel.: +81 03-5463-0642; fax: +81 03-5463-0642.
   E-mail address: vdekov0@kaiyodai.ac.jp (V.M. Dekov).

Production and hosting by Elsevier

reduction and methanogenesis, that take place above and below the sulfate-methane transition, respectively. The major part of V, Co, Ni, Cu, Zn, Cr, Mo, Cd and Sb is inferred to have co-precipitated with Fe in the euxinic deep waters and to have been incorporated into authigenic Fe-sulfides. Basin reservoir effect additionally influences the Mo enrichment. The U enrichment is interpreted to have a different origin in the two organic-rich stratigraphic units (II and I). It is inferred to be: (i) at the expense of the U inventory of the deepwater pool and a result of inorganic reduction of U at euxinic conditions in the lower Unit II; and (ii) at the expense of the U inventory of the surface water pool and a result of biogenic uptake and transfer to the sediment by the plankton in the upper Unit I. The high field strength elements are closely linked to the detrital component and their depletion in the organic-rich sediments reflects a dilution of the detrital component by the biogenic one. The enrichments of REE, Sn and Th are likely controlled by adsorption on clay minerals. Sr-Nd-Pb isotope compositions of the alumino-silicate component of the studied sediments are relatively uniform. They are most likely controlled by riverine suspended matter supplied mainly in the NW Black Sea (Danube Delta) and transported southward by marine currents, and to a lesser degree by suspended matter from the small rivers draining SE Bulgaria and NW Turkey. Wind-blown dust from the Sahara Desert appears to have a minor contribution to the alumino-silicate component of the sediments. The slight shift in the Pb isotopes in Unit I upper layers is possibly caused by the addition of anthropogenic Pb.

1. Introduction

The upper section of the sediment blanketing the Black Sea floor has been increasingly investigated since the first half of 20th century with the major goal to untangle the oceanographic/limnological as well as the geological history of this semi-isolated anoxic basin. The early works (Arkhangel'skii and Strakhov, 1938) subdivided it into three stratigraphic units (from top to bottom): (1) Recent sediments, (2) Old Black Sea layers, and (3) New Euxinian sediments. Later studies (Degens and Ross, 1972; Ross et al., 1970; Ross and Degens, 1974) essentially confirmed the presence of the same units (named as Units I, II and III), dated precisely their boundaries and showed that the stratigraphic units recognized at the shelf (Neveskii, 1967) are difficult to be correlated to those described in the deep Black Sea (Degens and Ross, 1972). Deep probing of the sediment and wide set of applied analytical approaches (Degens and Ross, 1974; Hsü, 1978; Ross, 1978; Ross et al., 1978; Stoffers and Müller, 1978; Stoffers et al., 1978) provided evidence that the distinct sediment alternation (Units I, II and III) records varying oxic lacustrine and anoxic marine conditions produced in the basin by the climatic changes over the Quaternary. Unraveling the Black Sea geological history and the potential implications for the processes in ancient anoxic basins involved the use of geochemical proxies (Calvert and Batchelor, 1978; Hirst, 1974). Geochemical studies of the Quaternary Black Sea sediments revealed that a number of trace elements are enriched (relative to the background detrital sediment or to the average shale) in the sediment layers deposited under anoxic conditions. They suggested that these enrichments may be used for determining the redox conditions in the sediment or in the bottom waters at the time of deposition (Calvert and Pedersen, 1993; Little et al., 2015). Although these studies comprehensively investigated the element enrichments and reasonably interpreted them as results of a range of reactions across redox interfaces (Calvert and Pedersen, 1993; Little et al., 2015) they considered only a limited number of elements (Cd, Cr, Cu, Fe, Mn, Mo, Ni, Re, U, V, Zn) measured in the uppermost (or uppermost + underlying; unclear in Little et al. (2015)) stratigraphic unit.

Challenged by the possibility to explore the environmental potential of a larger element set analyzed across the three Upper Quaternary stratigraphic units we investigated the distribution and enrichment of a large element set (54 elements) in a series of Holocene sediments from the western Black Sea. Since the upper organic-rich stratigraphic units (I and II) were shown to have received almost constant organic flux diluted by fluctuating terrigenous input through time (Calvert and Karlin, 1998) we, additionally, analyzed the Sr-Nd-Pb-isotope composition of the terrigenous component of these sediments in order to determine its provenance. The results of our study are discussed in this contribution.

2. Geologic setting

The Black Sea is the largest permanently anoxic basin in the modern Ocean. Permanent anoxia in the major part of its water body is a result of the combination of restricted water mass exchange with the Mediterranean Sea, positive water balance and moderate bio-production in the euphotic layer. The Black Sea water body is vertically stratified in two layers with contrasting chemistry that are separated by a transition layer (chemocline): oxic surface layer (∼0 to 50 m), suboxic intermediate/transition layer (chemocline) (∼50 to 100 m) and anoxic (euxinic) deep waters (∼100 to 2000 m) (Murray et al., 1989).

The upper part of the Black Sea sedimentary cover, deposited during the Late Pleistocene and Holocene, is composed of three distinct stratigraphic layers (units) spread throughout the deep Black Sea (Degens and Ross, 1972;
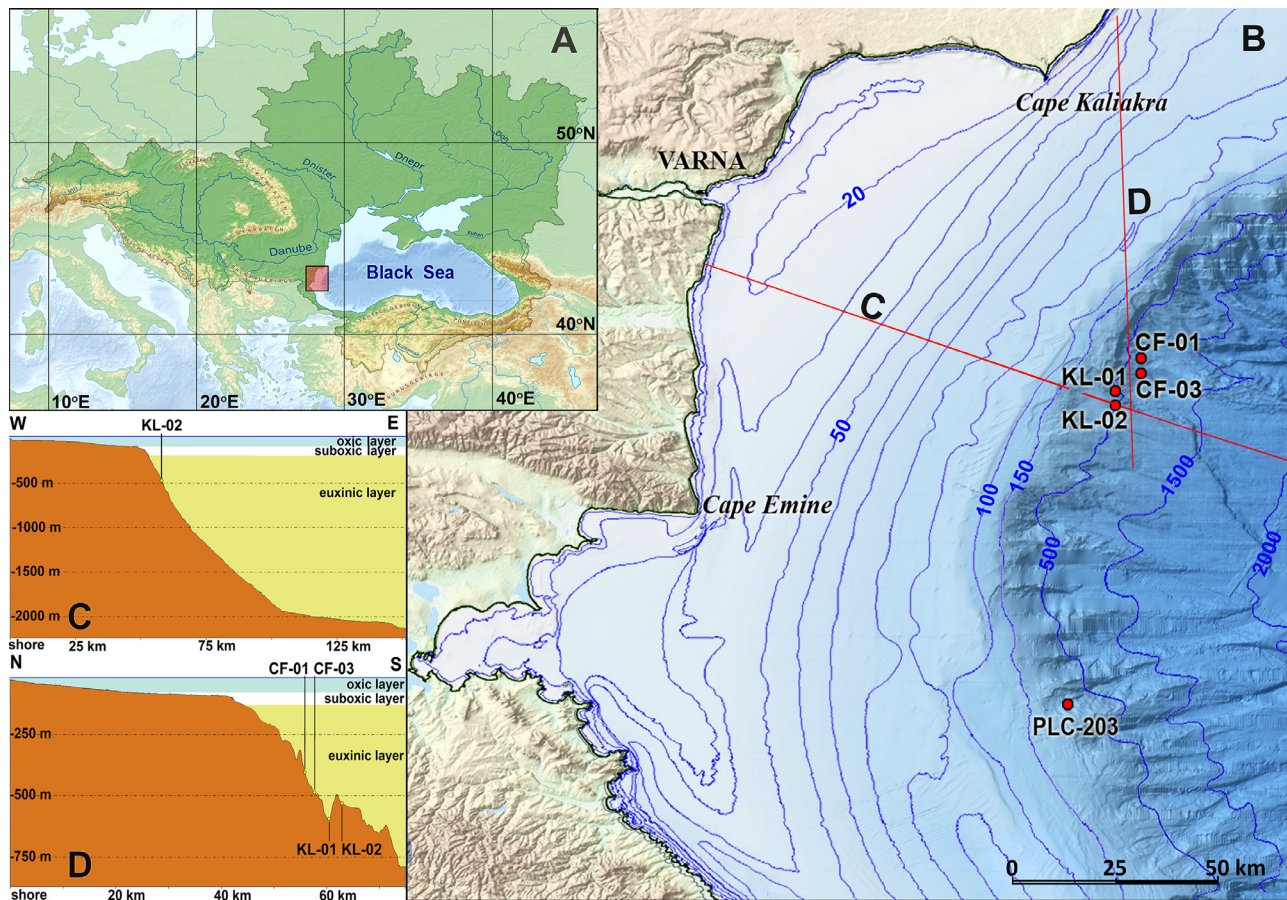
Figure 1 (a) Map of the Black Sea and its catchment area. Highlighted rectangle encircles the area of studies. (b) Western part of the Black Sea with locations of the studied sediment cores (red closed circles). Red lines marked with C and D indicate positions of the cross sections shown at (c) and (d) demonstrating the locations of the studied sediment cores CF-01, CF-03, KL-01 and KL-02 relative to the oxic, suboxic and euxinic water layers.

Ross et al., 1970). The uppermost layer (Unit I) is a modern laminated coccolith ooze that overlies the finely laminated sapropel (Unit II). The boundary between them is sharp and dated at ∼3 ka BP (Kwiecien et al., 2008). The transition between Unit II and Unit III, terrigenous mud (lutite; Ross et al., 1970), is distinct and estimated to be at ∼9 ka BP (Soulet et al., 2011). The deposition of these three different lithologic units is explained by changes in the environmental conditions, i.e. evolution of the basin from limnic to marine (Degens and Ross, 1972), whereas their impressive correlation along the entire basin is supposed to attest for uniform depositional environment over most of the Black Sea (Ross et al., 1970).

The organic-rich sapropel layer (Unit II) has been the focus of a number of studies (Calvert, 1990; Calvert et al., 1987; Glenn and Arthur, 1985). The high content of organic matter in this layer has been found to be caused by low dilution of the organic fraction by other sediment components (e.g., terrigenous and biogenic) rather than by high preservation of organic matter (Calvert and Karlin, 1998). Therefore, its formation is supposed not to be necessarily characteristic of anoxic basins. However, the anoxic conditions in the Black Sea water body and the deposition of organic-rich sediments (Units I and II) on the Black Sea floor were inferred to be the major controls of enrichment of a number of elements in the sediments (Calvert and Pedersen, 1993; Little et al., 2015).

3. Samples and methods of investigation

3.1. Samples

Five sediment cores recovered from the western deep Black Sea (Fig. 1a,b; Table 1) during two expeditions of the r/v *Akademik* (Institute of Oceanology, Bulgarian Academy of Sciences) in April 2006 and February 2007 were selected for our study. Twenty-nine sediment samples from the three stratigraphic units crossed by these cores (Unit III was not completely penetrated by any core) were washed from pore water salts with distilled water (18.2 MΩ/cm resistivity), freeze-dried and ground to fine powder in agate mortar before the elemental concentrations and isotope ratios measurements. The "red layers" in Unit III (Bahr et al., 2005; Kwiecien et al., 2008; Major et al., 2002) that mark the transition from the last glacial (Late Pleistocene) to Holocene were not reached by any core. Therefore, we can consider that the cored sediments are entirely within the Holocene.

Table 1　Investigated sediment cores sampling and lithology details.

Core ID	Latitude (N)	Longitude (E)	Depth (m)	Sampling device	Lithology description
CF-01	42°55.613′	28°36.405′	614	gravity corer	0—87 cm: finely laminated greenish-gray coccolith ooze (Unit I) 87—204 cm: finely laminated sapropel (Unit II) 204—223 cm: greenish-yellow fine terrigenous mud (Unit III)
CF-03	42°55.125′	28°36.413′	647	gravity corer	0—33 cm: finely laminated green-gray coccolith ooze (Unit I) 33—173 cm: finely laminated brown-green sapropel with sharp upper boundary (Unit II) 173—175 cm: sharp boundary 175—250 cm: grayish-white fine terrigenous mud (Unit III)
KL-01	42°52.505′	28°33.885′	457	gravity corer	0—94 cm: finely laminated greenish-gray coccolith ooze (Unit I) 95—210 cm: finely laminated (alternation of dark-brown organic-rich laminae and light-gray terrigenous laminae) sapropel (Unit II) 210 cm: sharp boundary 210—360 cm: greenish-gray fine terrigenous mud, with black stains (275-360 cm), which becomes compact down core (350—360 cm) (Unit III)
KL-02	42°53.045′	28°33.899′	475	gravity corer	0—115 cm: finely laminated greenish-gray coccolith ooze (Unit I) 115—250 cm: finely laminated brown to gray sapropel (Unit II) 250—320 cm: gray terrigenous mud (Unit III)
PLC-203	42°24.157′	28°27.796′	314	gravity corer	0—115 cm: finely laminated greenish-gray coccolith ooze (Unit I) 115—310 cm: sapropel (fine alternation of dark-brown to olive organic-rich laminae becoming denser towards the catch-corer, greenish-gray terrigenous laminae and rarely aragonite-rich laminae) (Unit II)

3.2. Methods of investigation

3.2.1. Bulk geochemical analyses and enrichment factors (EF) calculations

Major element (Al_2O_3, Fe_2O_3, MnO, MgO, CaO, Na_2O, K_2O, TiO_2, P_2O_5) concentrations of the samples were determined by Inductively Coupled Plasma Optical Emission Spectrometry (ICP-OES) (Spectro Ciros SOP instrument; Institute of Geosciences, University of Kiel) after total sample dissolution performed by pressurised HF-$HClO_4$-aqua regia attack (Garbe-Schönberg, 1993). Total SiO_2 (SiO_{2tot}) was estimated as the difference between the sum of all major elements including loss on ignition (LOI) and 100%. Amorphous SiO_2 (SiO_{2am}) concentrations were measured after sample dissolution following the method of DeMaster (1981) and Koning et al. (2002). About 20 mg of powdered sample was dissolved in 50 mL 0.5M NaOH in centrifuge tubes at 85°C for 3 hours (in a water-bath with stirring). After 1, 2 and 3 hours we centrifuged the tubes with dissolved samples (for 3 minutes at 3500 rpm), pipetted 0.5 mL from the solution, diluted this aliquot by 20 with distilled water (18.2 MΩ/cm resistivity) and analyzed it for dissolved silica using a Bran+Luebbe AA3 HR auto-analyzer as described

by Aminot and Kérouel (2007). Detrital SiO_2 (SiO_{2det}) concentrations were calculated by subtracting of SiO_{2am} from SiO_{2tot}.

Trace (Li, Sc, V, Cr, Co, Ni, Cu, Zn, Ga, Rb, Sr, Y, Zr, Nb, Mo, Ag, Cd, Sn, Sb, Cs, Ba, Hf, Ta, W, Tl, Pb, Th, U) and rare earth (REE) elements concentrations were analysed by Inductively Coupled Plasma Mass Spectrometry (ICP-MS) (Agilent 7500cs instrument; Institute of Geosciences, University of Kiel) after total sample dissolution following the same protocol as for the major elements (Garbe-Schönberg, 1993). Unfortunately, this dissolution protocol bears the risk of incomplete dissolution of some well-crystallized zircon grains and leaves a possibility that not all Zr and Hf are represented in the analysis. However, Zr, Hf and Nb, Ta, Th in the reference material Marine Sediment GSMS-2 (Jochum et al., 2005) that had been repeatedly analyzed together with our samples were recovered with 90% and 100%, respectively, and the observed perfect correlation between these elements and Al confirmed that a significant fraction of these high-field-strength elements (HFSE) had been dissolved and analyzed, which allowed for correct interpretations. The accuracy of the analytical results was controlled by analyzing international standard reference mate-

rials (AC-E, BE-N, BHVO-1, BHVO-2, BIR-1, MESS-2, GSMS-2) following the same analytical protocols as for the sediment samples. Measured elemental concentrations of the standards were generally within <5% of the recommended values for most elements. The precision of sample duplicates, as well as repeated analyses, was better than 5% for most elements.

Approximately 3—4 mg of each sample were loaded into tin capsules and placed in a 50-position automated Zero Blank sample carousel on a Carlo Erba NA1500 CNHS elemental analyzer for measuring the total carbon (C_{tot}) and nitrogen concentrations. After flash combustion in a quartz column containing chromium oxide and silvered cobaltous/cobaltic oxide at 1020°C in an oxygen-rich atmosphere, the sample gas was transported in a He carrier stream and passed through a hot (650°C) reduction column consisting of reduced elemental copper to remove oxygen. The effluent stream then passed through a chemical [$Mg(ClO_4)_2$] trap to remove water. The stream then passed through a 0.7 meter GC column at 125°C that separates the N_2 and CO_2 gases. Finally, the gases passed through a thermal conductivity detector that measured the size of the pulses of N_2 and CO_2.

Total inorganic carbon (C_{inorg}) was measured coulometrically using a UIC (Coulometrics) 5014 CO_2 coulometer coupled with an AutoMate automated carbonate preparation device (AutoMateFX.com). Approximately 20 mg of each sample was weighed into septum top tubes and placed into the AutoMate carousel. A double needle assembly was used to purge the sample vial of atmospheric gas using CO_2-free nitrogen carrier gas. 10% phosphoric acid was then injected into the sample vial and evolved CO_2 was carried through a silver nitrate scrubber to the coulometer where C content was measured.

Organic carbon (C_{org}) concentrations were calculated as a difference between the measured total carbon and total inorganic carbon concentrations.

LOI (in wt.%) was measured on air-dry powdered samples placed after weighing in a muffle furnace at 950°C for 1 hour.

In order to evaluate the relative enrichment or depletion of the elements in the sediment we calculated the authigenic enrichment factors (Calvert and Pedersen, 1993; Little et al., 2015):

$$EF_{element} = (element/Al)_{sample}/(element/Al)_{reference}.$$

Traditionally, the reference material for normalization was the average shale (Calvert and Pedersen, 1993). Little et al. (2015) argued that the average shale could not be representative of the local background sedimentation and suggested the usage of the proximal oxic sediment as a correct normalizing lithogenic background. Since we have not studied the composition of the proximal shelf sediments (oxic and detrital) contemporaneous with the studied deep-sea stratigraphic units (Unit I, II and III) we normalized our concentration data to those for the upper continental crust (UCC) (Rudnick and Gao, 2003).

3.2.2. Sr-Nd-Pb isotope analysis

Twenty-three sub-samples (out of the entire set of 29) from four of the sediment cores were selected for a combined Sr-Nd-Pb isotope study (Department of Geological Sciences,

Swedish Museum of Natural History, Stockholm). According to previous works (Ross et al., 1970; Ross and Degens, 1974) the Upper Pleistocene-Holocene Black Sea sediments (Units III—I) contain a considerable proportion of biogenic carbonate and organic matter. These sediment components are marine-born and their Sr-Nd-Pb-isotope composition is supposed to reflect that of the seawater (Haley et al., 2008; Hedge and Walthall, 1963; Vance and Burton, 1999). Thus, in order to trace the provenance of the non-marine component (e.g., terrigeneous) in the studied sediments we subjected the selected sub-samples to a three-step leaching procedure (Bayon et al., 2002) to eliminate the marine-born components. First, 10% acetic acid was added to ~150 mg of the powdered sample which, after 3 hours in an ultrasonic bath, was left overnight. This treatment step removes the carbonates. After rinsing with distilled water (18.2 MΩ/cm resistivity), centrifugation, and decantation the residue was collected. Second, Fe-Mn-oxyhydroxides were removed from the residue by adding 25% acetic acid, with sample vials left on a hot plate kept at different temperatures (at 90° and 60°C) for a total period of two hours. After rinsing with distilled water, centrifugation and decantation, the residue was recovered. Third, the organic carbon was removed from the residues by adding 5% H_2O_2 to them and keeping the vials for seven hours in an ultrasonic bath. In order to ensure that the organic fraction was fully dissolved, we added aqua regia to the vials. The final residue (after rinsing, centrifugation and decantation) is supposed to represent the alumino-silicate fraction of the sediment. In order to estimate the quantity of different fractions during the treatment, the resulting sample residues were weighed. We found that the alumino-silicates compose ~40—60% of the studied sediment samples.

The alumino-silicate residues were dissolved in a HF-$HClO_4$ acid mixture before the Sr-Nd-Pb-isotope ratio measurements. The sample solutions were left for three days in order to ensure the total dissolution of the alumino-silicate component. Conventional ion-exchange techniques, performed in columns filled with AG50W × 8, H^+ form resin (De Ignacio et al., 2006), were applied to the sample solutions in order to separate and purify the elements whose isotopic composition were to be determined. Sr was further purified in a second pass through the same columns, whereas Nd was isolated in Ln-spec columns (Pin and Zalduegui, 1997). The Pb fractions were re-dissolved in HBr, and treated further in columns with AG1 × 8, Cl^- form resin.

A Thermo-Finnigan Triton thermal ionization mass spectrometry (TIMS) instrument was used for the Sr and Nd isotope analyses and data were normalized to $^{88}Sr/^{86}Sr = 0.1194$ and $^{146}Nd/^{144}Nd = 0.7219$, respectively. Additionally, replicate analyses of the NBS-987 Sr standard analyzed during the course of the study yielded an average $^{87}Sr/^{86}Sr = 0.710221 \pm 0.000011$ (2σ external precision). Corresponding analyses of the La Jolla Nd standard yielded an average $^{143}Nd/^{144}Nd = 0.511848 \pm 0.000009$ (2σ external precision). These standard values are very close to the accepted values and therefore, no additional corrections were applied to the obtained sample Sr or Nd data. Estimated analytical uncertainties amount to ca. ± 0.4 and ± 0.00002 for the given εNd and Sr isotope values, respectively. Pb isotope analyses were performed with Tl added to allow for an internal correction of the mass bias, and the

measured intensities were corrected for background and Hg interference on mass 204. Two ICP-MS instruments were used: a Micromass Isoprobe multi-collector (core KL-02) and a Nu Plasma II (cores CF-03, KL-01 and PLC-203). For the data produced by the latter instrument (hosted by the Vegacenter facility), the NBS-981 Pb standard was run at regular intervals and all unknowns were analyzed in duplicate. The obtained values for the standard are within the error of those given by Todt et al. (1996), and the external reproducibility is between 0.04% (^{206}Pb/^{204}Pb) and 0.08% (^{208}Pb/^{204}Pb). The external reproducibility of the unknowns is of a similar order, but in order to account for errors arising during the chemical treatment in the clean laboratory, an overall uncertainty of $\pm 0.10\%$ is adopted.

4. Results

4.1. Geochemistry of the sediments

4.1.1. Elemental concentrations and REE distribution patterns

Vertical distributions of the concentrations of Al, Fe and K co-vary along the studied sediment cores (Table 2; Fig. 2). Titanium and detrital SiO$_2$ co-vary with them in the upper part of Unit II and in Unit I (Fig. 2). Concentrations of Si (total, detrital and amorphous), Al, Fe and K have maximum values in the sapropel layer (Unit II) and minimum values in the terrigenous mud (Unit III) and coccolith ooze (Unit I) (Table 2). Calcium (as CaCO$_3$) demonstrates opposite behavior with maximum concentrations in both the terrigenous mud and coccolith ooze, and minimum content in the sapropel layer (Table 2; Fig. 2). Although the content of Mn is broadly similar in all the three stratigraphic units (Table 2) it shows a particular vertical distribution with a gradual increase from Unit III towards the boundary between Units II and I, followed by a slight decrease through Unit I (Fig. 2). Unit I has the lowest Mg and the highest P concentrations (Table 2). Organic carbon shows the highest content in the sapropel layer (particularly in its lower part) and lowest concentration in the terrigenous mud (Table 2; Fig. 2). It correlates well with SiO$_{2am}$ (Table 2; Fig. 2).

Silicon, Al and Ca appeared to be the most abundant major elements in these sediments (Table 2). Theoretically, Al is mostly terrigenous (detrital), whereas Si has a dual origin, terrigenous and biogenic, in these sediments (Hay et al., 1990). Biogenic Si concentrations (within the amorphous SiO$_2$ of diatoms and silicoflagellates (Pilskaln and Pike, 2001)) cluster between 1 and 2% (as SiO$_{2am}$) and have a maximum in the sapropel layer (Table 2). In order to investigate the terrigenous material deposited in the western Black Sea during the Holocene, we calculated the SiO$_{2det}$/Al$_2$O$_3$ ratio in the studied sediments (Table 2). This ratio spans between 4.5 and 7.8, but clusters around 5 (Table 2). Assuming that the terrigenous material entering the western Black Sea has an average composition close to that of the UCC, we compared the SiO$_{2det}$/Al$_2$O$_3$ ratio of our sediments to that of the UCC: 4.3 (Rudnick and Gao, 2003). This comparison demonstrated that the western Black Sea sediments are enriched in SiO$_{2det}$ relative to the UCC.

Vertical distributions of the concentrations of most trace elements co-vary with those of one or another of the major elements. A large group of trace elements including Li, Co, Ni, Cu, Zn, V, Cr, Ag, Sc, Ga, Sn, Rb, Cs, W, Th, Nb, Ta, Hf and REE correlate positively with Al (Fe and K) (Fig. 2). Similarly, Sr co-varies with CaCO$_3$, Ba with Mn, and Pb, Y with P (Fig. 2). Two pairs of trace elements do not show any correlation with the major elements, but co-vary with each other: Cd with Sb, and U with Mo (Fig. 2). Like most of the major elements a range of trace elements have maximum concentrations in the sapropel layer and minimum contents in the terrigenous mud: V, Cr, Ni, Cu, Zn, Cd, Ga, Mo, Sb, Li, Rb, Cs, Ba, Sn, Sc, Zr, Hf, Ta, W, Tl, Th, U and REE (Tables 2, 3). Co, Pb and Y have maximum concentrations in the coccolith ooze and minimum concentrations in the terrigenous mud (Tables 2, 3). Sr concentrations are also the highest in the coccolith ooze, but lowest in the sapropel layer (Table 2).

Concentrations of the REE (ΣREE) are the highest in the sapropel layer (Unit II) and the lowest in the terrigenous mud (Unit III) (Table 3; Fig. 3a). ΣREE correlates inversely with the SiO$_{2det}$/Al$_2$O$_3$ ratio (Tables 2, 3). The UCC-normalized REE distribution patterns of all the three stratigraphic units are similar (Fig. 3a). They show very weak negative to no Ce anomaly (Ce/Ce*$\sim$1), have a weak negative Eu anomaly (Eu/Eu*$<$1) and exhibit depletion of light REE relative to heavy REE (La$_{UCCN}$/Lu$_{UCCN}$$<$1) (Fig. 3a; Table 3). The negative Eu anomaly is highest in the terrigenous mud (Fig. 2).

4.1.2. Enrichment factors
Iron is enriched relative to Al in all the three stratigraphic units over the UCC abundance (Table 4). Although the Fe enrichment is, on average, similar in all stratigraphic units (Table 4) it varies along the sediment cores showing a general trend of upward decrease with two maxima at the lower and upper parts of Unit II, which is similar to the vertical profile of the C$_{org}$ concentrations (Figs 2, 4).

Organic-rich sediments are typically enriched in trace elements (Goldschmidt, 1954) and our data largely confirm this observation: most of the analyzed trace elements (Ag, V, Cr, Co, Ni, Cu, Zn, Cd, Ga, Mo, Sb, Li, Rb, Cs, Sr, Ba, Sn, Sc, Nb, Ta, W, Tl, Pb, Th, U, Y and REE) show elevated concentrations in the organic-rich Units I and II (some even in the terrigenous mud, Unit III) (Table 4). Others, such as Mn, Zr and Hf, are depleted in these sediments (Table 4). The sapropel layer (Unit II) is the most enriched in V, Cr, Ni, Cu, Zn, Cd, Mo, Sb, Li, Rb, Cs, Sc, Tl and U, whereas the coccolith ooze (Unit I) is the most enriched in Ag, Co, Ba, Pb, Y and Tm (Table 4). The terrigenous mud (Unit III) is the richest in Mn, Sr, Sn, Zr, Hf, Nb, Ta, W, Th and most of the REE (La, Ce, Pr, Nd, Sm, Eu, Gd, Tb, Dy, Lu) (Table 4). Particularly enriched (EF$>$3) are Mo, Cd, Ag, Sb, Li and U (Table 4).

The vertical profile of the EF$_{Mn}$ (Fig. 4) shows depletion in the sapropel layer (Unit II) and gradual increase upwards to the coccolith ooze (Unit I). The EF$_{Ba}$ shows a similar profile (Fig. 4), but its absolute minimum and maximum appear earlier than those of the EF$_{Mn}$: at the base and at the upper part of Unit II, respectively. Sr is strongly depleted in the sapropel layer (Unit II). The vertical profiles of the enrichment factors of Co and Cu co-vary with that of Fe (Fig. 4). The enrichments of Ni, Zn, W, Cr, Ga, Sc, Li and Cs (and Rb, not shown at Fig. 4) demonstrate maxima like that of EF$_{Fe}$ at the base of Unit II, but their upper (and smaller) maxima are displaced upward in Unit I (Fig. 4). EF$_V$, EF$_{Mo}$,

Table 2 Major and trace elements concentrations (measured using Inductively Coupled Plasma Optical Emission Spectrometry (ICP-OES) and Inductively Coupled Plasma Mass Spectrometry (ICP-MS)) of the studied sediments.

Core ID	Horizon (cm)	Lithology Unit	SiO_{2tot} (wt.%)	SiO_{2am}	SiO_{2det}	Al_2O_3	SiO_{2det}/Al_2O_3	Fe_2O_{3tot}	MnO	MgO	CaO	Na_2O	K_2O	TiO_2	P_2O_5	LOI	C_{inorg}	C_{org}	C_{tot}	N	Si_{am}/C_{org} (mol/mol)	Ag (ppm)	V
CF-01	57—59	I	48.7	0.77	47.9	8.88	5.4	3.58	0.05	1.85	11.3	1.39	1.64	0.37	0.12	22.1	2.80	2.64	5.44	0.26	0.06	0.18	100
	93—95	II	53.0	1.37	51.6	11.0	4.7	4.46	0.06	2.20	4.82	1.58	2.01	0.44	0.14	20.4	1.02	4.36	5.38	0.42	0.06	0.19	120
	124—126	II	52.3	1.27	51.0	10.3	4.9	4.12	0.05	2.28	5.88	1.48	1.89	0.44	0.10	21.2	1.24	3.97	5.21	0.37	0.06	0.17	120
	155—157	II	50.1	5.24	44.9	7.83	5.7	3.14	0.04	1.83	4.16	2.27	1.39	0.30	0.14	28.9	0.99	7.25	8.24	0.60	0.14	0.15	107
	195—197	II	47.8	0.89	46.9	7.77	6.0	3.02	0.03	1.83	7.07	1.24	1.43	0.31	0.13	29.3	2.25	7.05	9.30	0.51	0.03	0.16	159
	218—220	III	50.8	0.84	49.9	8.50	5.9	3.36	0.04	2.45	11.5	1.36	1.60	0.41	0.10	19.8	2.61	1.89	4.50	0.15	0.09	0.12	87.3
CF-03	55—57	II	52.3	1.67	50.6	10.2	5.0	4.09	0.05	2.30	5.52	1.99	1.89	0.42	0.13	21.1	1.24	4.29	5.53	0.39	0.08	0.17	117
	104—106	II	52.0	1.32	50.7	10.6	4.8	4.08	0.04	2.13	5.08	1.47	1.91	0.42	0.13	22.1	1.12	4.87	5.99	0.43	0.05	0.18	128
	133—135	II	49.5	1.91	47.6	8.91	5.3	3.57	0.04	1.96	4.80	1.49	1.61	0.35	0.12	27.6	1.03	7.79	8.82	0.67	0.05	0.17	120
	170—172	II	55.6	0.67	55.0	7.78	7.1	2.93	0.03	2.03	6.28	1.45	1.42	0.35	0.12	22.0	1.34	4.27	5.61	0.28	0.03	0.14	119
	216—218	III	39.1	0.64	38.5	4.91	7.8	1.99	0.04	1.63	21.2	0.62	0.90	0.21	0.07	29.3	6.40	1.10	7.50	0.08	0.12	0.08	55.7
KL-01	165—167	II	51.3	1.42	49.9	9.49	5.3	3.80	0.05	2.10	4.74	1.57	1.73	0.38	0.11	24.7	1.12	6.87	7.99	0.62	0.04	0.17	116
	178—180	II	50.1	1.28	48.9	9.51	5.1	3.88	0.04	2.06	4.85	1.58	1.75	0.37	0.10	25.7	1.03	6.80	7.83	0.54	0.04	0.16	120
	200—202	II	48.4	0.88	47.5	8.66	5.5	3.41	0.03	2.00	7.41	1.39	1.60	0.34	0.10	26.6	1.71	6.13	7.84	0.48	0.03	0.15	131
	250—252	III	40.3	0.59	39.7	5.25	7.5	2.12	0.05	1.69	22.6	0.75	0.98	0.22	0.07	26.0	6.47	1.10	7.57	0.08	0.11	0.08	57.6
	294—296	III	40.9	1.41	39.5	5.82	6.8	2.28	0.04	1.77	16.5	0.72	1.06	0.26	0.09	30.5	4.94	1.31	6.25	0.10	0.21	0.10	65.9
KL-02	58—60	I	47.0	0.80	46.2	8.70	5.3	3.39	0.05	1.72	12.2	1.28	1.58	0.35	0.11	23.6	3.21	2.57	5.78	0.26	0.06	0.16	107
	86—88	I	47.7	1.00	46.7	8.64	5.4	3.44	0.05	1.78	12.1	1.26	1.59	0.35	0.13	22.9	3.23	2.82	6.05	0.28	0.07	0.18	104
	116—118	II	53.2	1.39	51.8	11.5	4.5	4.65	0.06	2.34	4.75	1.43	2.09	0.47	0.11	19.4	0.94	4.03	4.97	0.38	0.07	0.21	136
	153—155	II	52.1	1.55	50.5	10.4	4.8	4.12	0.05	2.28	5.69	1.37	1.91	0.43	0.11	21.5	1.24	4.23	5.47	0.39	0.07	0.18	122
	204—206	II	51.9	7.40	44.5	8.91	5.0	3.51	0.04	2.00	4.73	1.66	1.62	0.36	0.10	25.1	0.92	6.26	7.18	0.53	0.24	0.15	109
	232—234	II	50.5	1.17	49.3	9.43	5.2	3.91	0.04	2.13	4.92	1.66	1.74	0.38	0.11	25.2	1.18	6.66	7.84	0.53	0.04	0.15	130
	270—272	III	50.9	0.88	50.0	8.36	6.0	3.41	0.05	2.44	12.1	1.08	1.55	0.41	0.10	19.6	2.99	1.74	4.73	0.13	0.10	0.12	84.6
PLC-203	65—67	I	49.3	1.73	47.6	9.46	5.0	3.82	0.07	1.94	10.8	1.21	1.73	0.40	0.13	21.2	2.72	2.53	5.25	0.25	0.14	0.16	113
	109—111	I	50.2	1.27	48.9	10.1	4.9	4.00	0.06	2.14	9.12	1.39	1.86	0.42	0.11	20.7	2.35	2.26	4.61	0.22	0.11	0.17	120
	170—172	II	53.4	2.27	51.2	11.3	4.5	4.59	0.06	2.41	4.80	1.26	2.06	0.47	0.12	19.5	0.91	3.34	4.25	0.32	0.14	0.17	126
	218—220	II	52.3	2.62	49.7	10.6	4.7	4.44	0.06	2.33	4.87	1.39	1.96	0.45	0.11	21.4	0.91	3.69	4.60	0.34	0.14	0.16	117
	260—262	II	54.0	1.92	52.1	10.9	4.8	4.40	0.04	2.36	5.46	1.26	1.98	0.45	0.11	19.0	1.06	3.69	4.75	0.35	0.10	0.17	120
	278—280	II	51.0	2.79	48.2	9.66	5.0	4.08	0.06	2.18	5.00	1.25	1.77	0.40	0.11	24.6	0.85	5.11	5.96	0.46	0.11	0.16	112
Average		I	48.6	1.11	47.5	9.15	5.2	3.65	0.06	1.89	11.1	1.30	1.68	0.38	0.12	22.1	2.86	2.56	5.43	0.25	0.09	0.17	109
		II	51.6	2.05	49.6	9.72	5.1	3.91	0.05	2.14	5.31	1.52	1.78	0.40	0.12	23.4	1.16	5.30	6.46	0.45	0.08	0.17	123
		III	44.4	0.87	43.5	6.57	6.6	2.63	0.04	2.00	16.8	0.90	1.22	0.30	0.09	25.0	4.68	1.43	6.11	0.11	0.12	0.10	70.2

Table 2 (*continued*)

| Core ID	Horizon (cm)	Lithology Unit	Cr (ppm)	Co	Ni	Cu	Zn	Cd	Ga	Mo	Sb	Li	Rb	Cs	Sr	Ba	Sn	Sc	Zr	Hf	Nb	Ta	W	Tl	Pb	Th	U
CF-01	57—59	I	80.6	17.0	64.7	38.7	73.9	0.44	13.8	47.1	1.60	51.9	104	7.08	520	573	2.21	11.6	64.8	1.86	8.75	0.61	1.17	0.64	26.6	8.42	9.73
	93—95	II	101	19.1	79.3	54.8	91.2	0.54	17.4	56.7	1.30	65.6	127	8.73	239	720	2.64	15.1	78.1	2.25	10.3	0.72	1.33	0.71	22.5	10.0	6.97
	124—126	II	100	14.0	78.6	41.5	87.0	0.60	16.7	61.9	1.67	60.6	122	8.31	254	560	2.65	13.9	74.9	2.15	10.5	0.73	1.39	0.82	20.9	9.93	12.8
	155—157	II	84.2	14.3	84.3	45.4	77.0	0.64	14.0	41.7	1.17	50.5	101	7.10	218	429	2.20	12.0	55.1	1.64	8.07	0.57	1.20	0.62	17.7	8.09	12.4
	195—197	II	76.9	11.2	77.0	47.6	71.7	0.66	13.8	71.1	1.36	47.6	101	6.76	534	412	2.17	11.2	62.5	1.80	8.22	0.59	1.21	0.89	18.0	8.26	15.1
	218—220	III	76.1	10.4	43.8	26.8	66.2	0.29	13.4	5.15	1.23	43.0	92.2	5.69	303	421	2.31	10.0	62.1	1.83	9.34	0.67	1.21	0.54	15.9	8.33	3.29
CF-03	55—57	II	97.1	15.0	75.3	43.5	87.1	0.63	16.4	55.3	1.64	60.8	125	8.40	241	592	2.63	13.4	66.5	1.91	10.2	0.71	1.33	0.85	20.8	9.64	9.36
	104—106	II	99.7	14.9	84.2	49.7	91.1	0.76	17.1	67.1	1.66	63.9	126	8.84	245	766	2.57	14.1	78.5	2.26	10.1	0.70	1.33	0.80	21.6	9.89	13.9
	133—135	II	93.2	15.2	84.4	49.0	85.2	0.80	15.9	71.5	1.44	57.0	115	8.15	241	754	2.45	13.3	64.5	1.84	9.22	0.65	1.35	0.74	19.7	9.01	13.1
	170—172	II	72.6	9.59	62.4	38.1	61.8	0.62	12.2	34.4	1.31	40.9	85.7	5.42	270	378	2.01	9.61	62.7	1.81	8.38	0.60	1.11	0.86	15.1	7.33	9.31
	216—218	III	46.6	6.69	30.3	18.1	42.1	0.23	8.61	1.04	0.71	29.2	58.8	3.86	451	284	1.45	6.68	35.9	1.13	5.46	0.40	0.75	0.38	10.2	5.38	2.07
KL-01	165—167	II	96.34	14.6	78.9	46.3	84.4	0.60	16.0	62.6	1.23	57.8	121	8.39	203	476	2.56	13.1	62.3	1.81	9.65	0.68	1.32	0.69	20.3	9.37	12.3
	178—180	II	96.75	16.9	83.4	43.7	84.9	0.82	16.3	159	1.81	59.6	124	8.58	220	400	2.58	13.2	59.4	1.74	9.42	0.66	1.32	0.74	20.0	9.30	19.7
	200—202	II	86.34	12.9	83.1	42.6	78.5	0.64	14.9	109	1.78	53.1	110	7.68	682	367	2.36	12.1	60.6	1.76	8.72	0.61	1.24	0.74	18.9	8.80	21.3
	250—252	III	50.29	7.32	32.2	16.7	43.0	0.22	8.89	0.78	0.65	29.5	59.7	4.01	436	231	1.49	6.99	38.2	1.18	5.61	0.40	0.77	0.38	10.4	5.41	1.86
	294—296	III	56.63	7.80	36.1	18.3	49.7	0.24	10.3	0.77	0.62	33.8	69.2	4.44	383	263	1.76	7.92	47.2	1.42	66.86	0.49	0.90	0.42	12.1	6.46	2.42
KL-02	58—60	I	79.0	15.7	64.1	42.2	73.2	0.62	14.0	45.7	1.61	52.2	104	7.04	574	471	2.21	11.6	60.3	1.79	8.39	0.59	1.11	0.70	19.8	8.20	9.40
	86—88	I	80.9	16.3	69.0	41.8	75.2	0.50	14.1	35.7	1.13	52.4	106	7.19	580	551	2.29	11.8	59.8	1.75	8.76	0.61	1.15	0.72	26.4	8.51	7.18
	116—118	II	107	25.0	87.3	60.7	96.5	0.65	18.1	45.3	1.54	67.1	130	9.17	229	856	2.75	15.1	76.1	2.21	10.7	0.75	1.37	0.78	22.6	10.4	6.17
	153—155	II	97.9	15.1	75.1	43.5	86.1	0.59	16.8	46.0	1.27	61.5	126	8.57	249	719	2.63	13.7	72.2	2.11	10.4	0.73	1.34	0.90	21.5	9.87	7.33
	204—206	II	91.9	14.5	72.3	43.3	77.8	0.54	15.2	81.5	1.19	55.1	112	7.91	217	416	2.38	12.6	58.2	1.73	9.05	0.64	1.23	0.68	18.8	8.86	10.3
	232—234	II	96.5	18.7	94.2	42.9	83.2	0.64	16.1	112	1.86	56.5	119	8.23	223	366	2.57	13.1	66.0	1.92	9.61	0.68	1.38	0.70	20.3	9.42	10.6
	270—272	III	73.8	10.8	49.0	23.1	63.4	0.30	13.0	2.62	1.12	42.6	89.3	5.46	310	348	2.25	9.78	60.5	1.79	9.32	0.68	1.18	0.52	15.8	8.14	3.13
PLC-203	65—67	I	91.6	17.7	65.3	38.9	77.8	0.37	15.2	21.3	1.22	55.0	115	7.70	509	501	2.46	12.1	64.9	1.91	9.55	0.67	1.30	0.72	24.8	9.02	4.77
	109—111	I	91.1	17.3	64.9	37.6	81.2	0.35	15.5	20.0	1.40	57.4	116	7.93	396	569	2.52	12.5	60.8	1.81	9.72	0.68	1.27	0.77	23.1	9.07	3.88
	170—172	II	107	21.4	79.3	42.1	92.1	0.53	17.8	33.4	1.74	65.8	133	9.26	215	913	2.83	14.5	74.8	2.17	10.9	0.77	1.40	0.86	21.9	10.4	5.98
	218—220	II	108	20.6	78.1	36.6	92.1	0.43	17.2	33.9	1.16	62.2	131	9.22	200	433	2.73	13.8	69.7	2.03	10.7	0.75	1.39	0.80	21.9	10.0	5.18
	260—262	II	103	17.2	72.0	38.4	91.2	0.40	17.3	37.0	1.25	63.1	128	8.81	219	444	2.75	14.0	70.3	2.08	10.7	0.76	1.41	0.80	21.3	10.2	5.73
	278—280	II	101	18.1	75.4	40.1	88.4	0.45	16.4	55.2	1.59	59.2	120	8.41	205	433	2.64	13.5	70.1	2.05	10.2	0.72	1.42	0.72	20.4	9.73	6.49
Average		I	84.6	16.8	65.6	39.8	76.3	0.46	14.5	34.0	1.39	53.8	109	7.39	516	533	2.34	11.9	62.1	1.82	9.03	0.63	1.20	0.71	24.1	8.64	6.99
		II	95.6	16.2	79.2	44.7	84.6	0.61	16.1	65.0	1.47	58.3	119	8.21	269	549	2.53	13.2	67.5	1.96	9.74	0.69	1.32	0.77	20.2	9.39	10.7
		III	60.7	8.60	38.3	20.6	52.9	0.26	10.8	2.07	0.87	35.6	73.8	4.69	377	309	1.85	8.27	48.8	1.47	19.3	0.53	0.96	0.45	12.9	6.74	2.55
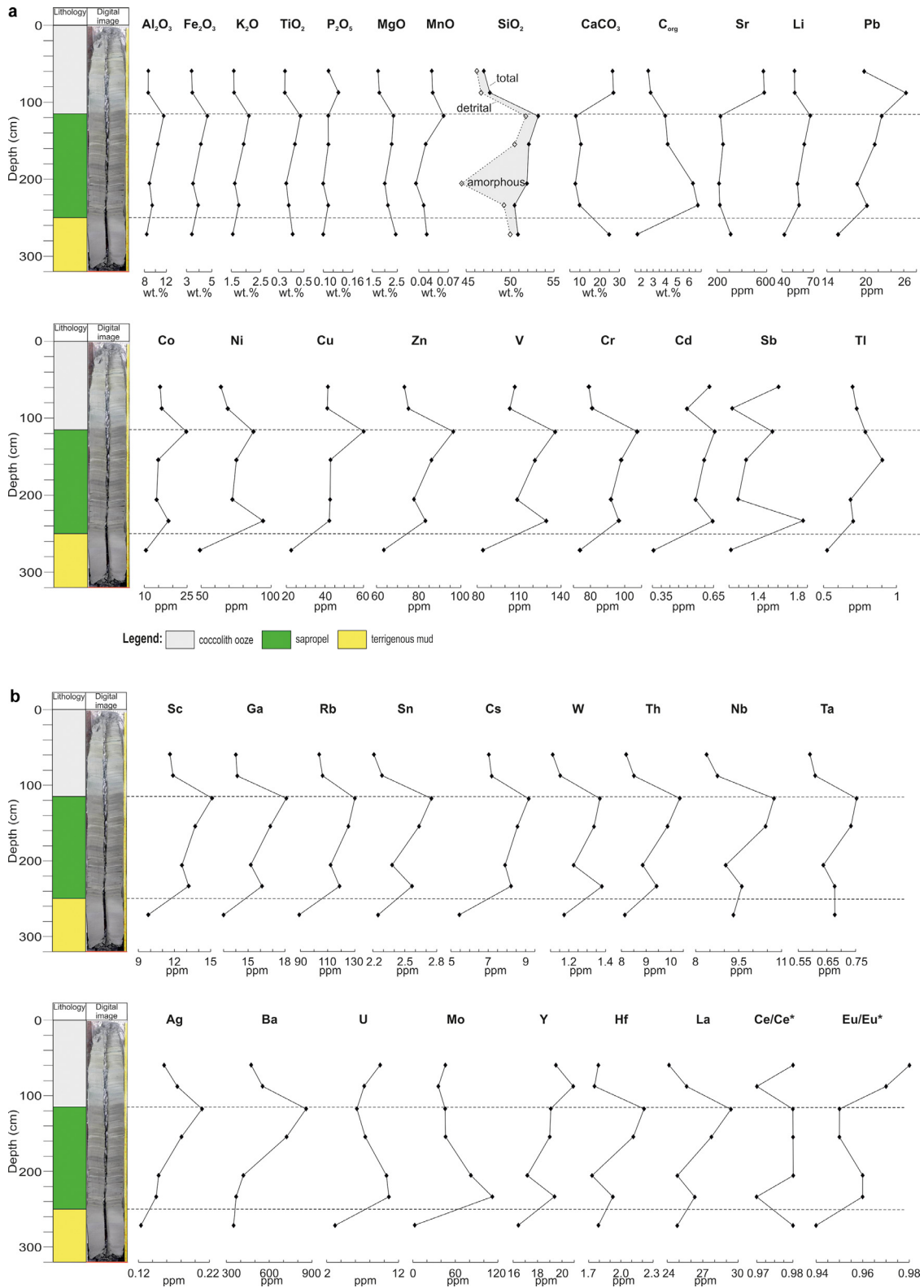
Figure 2 Vertical profiles of selected elements concentrations and selected elements ratios along the sediment core KL-02.

Table 3 Rare earth elements (REE) and Yttrium (Y) concentrations (measured using Inductively Coupled Plasma Mass Spectrometry, ICP-MS) of the studied sediments.

Core ID	Horizon (cm)	Lithology Unit	La (ppm)	Ce	Pr	Nd	Sm	Eu	Gd	Tb	Dy	Ho	Er	Tm	Yb	Lu	Y	ΣREE	(Ce/Ce*)[a]	(Eu/Eu*)[b]	La_{UCCN}/Lu_{UCCN}
CF-01	57—59	I	25.0	50.6	5.97	23.0	4.59	0.98	4.19	0.64	3.72	0.73	2.00	0.30	1.93	0.28	19.9	124	0.98	0.96	0.88
	93—95	II	28.9	58.6	6.83	25.9	5.13	1.07	4.50	0.69	3.98	0.78	2.15	0.32	2.15	0.32	20.5	141	0.98	0.96	0.90
	124—126	II	27.9	56.9	6.70	25.4	5.07	1.04	4.45	0.68	3.88	0.75	2.06	0.31	2.05	0.30	19.8	138	0.98	0.95	0.92
	155—157	II	22.9	46.1	5.45	21.1	4.25	0.90	3.96	0.61	3.56	0.71	1.98	0.30	1.96	0.30	20.1	114	0.97	0.95	0.77
	195—197	II	23.4	46.8	5.59	21.4	4.34	0.92	3.96	0.61	3.59	0.71	1.93	0.29	1.92	0.29	19.9	116	0.96	0.96	0.81
	218—220	III	25.3	51.7	6.10	23.3	4.60	0.93	3.96	0.60	3.38	0.66	1.79	0.26	1.75	0.26	17.4	125	0.98	0.94	0.97
CF-03	55—57	II	27.6	56.2	6.60	25.1	4.97	1.02	4.31	0.65	3.71	0.72	1.97	0.29	1.96	0.29	18.9	135	0.98	0.96	0.96
	104—106	II	27.8	56.1	6.58	24.9	4.90	1.01	4.29	0.66	3.83	0.75	2.09	0.31	2.10	0.31	19.9	136	0.98	0.96	0.89
	133—135	II	25.4	51.3	6.08	23.2	4.63	0.96	4.15	0.64	3.69	0.73	2.00	0.30	1.99	0.30	19.6	125	0.97	0.95	0.86
	170—172	II	22.2	44.4	5.34	20.5	4.08	0.86	3.67	0.56	3.22	0.63	1.74	0.26	1.71	0.25	17.3	109	0.96	0.96	0.88
	216—218	III	15.6	31.7	3.77	14.5	2.86	0.57	2.49	0.37	2.09	0.41	1.11	0.16	1.10	0.16	10.8	77	0.97	0.93	0.96
KL-01	165—167	II	26.4	53.8	6.34	24.1	4.79	1.00	4.19	0.64	3.65	0.71	1.94	0.29	1.91	0.28	18.6	130	0.98	0.96	0.93
	178—180	II	25.9	52.2	6.16	23.4	4.67	0.97	4.08	0.62	3.56	0.69	1.88	0.28	1.86	0.28	18.1	127	0.97	0.96	0.94
	200—202	II	24.7	49.8	5.93	22.7	4.54	0.95	4.11	0.62	3.57	0.69	1.89	0.28	1.85	0.28	18.8	122	0.97	0.95	0.90
	250—252	III	16.0	32.4	3.84	14.7	2.90	0.59	2.49	0.37	2.13	0.41	1.13	0.17	1.11	0.17	10.9	78	0.97	0.95	0.97
	294—296	III	20.1	40.9	4.80	18.3	3.57	0.70	3.05	0.45	2.51	0.48	1.30	0.20	1.29	0.19	12.7	98	0.98	0.92	1.06
KL-02	58—60	I	24.1	48.8	5.75	22.0	4.40	0.95	4.01	0.62	3.62	0.71	1.97	0.29	1.93	0.29	19.6	119	0.98	0.98	0.84
	86—88	I	25.6	51.7	6.10	23.5	4.74	1.01	4.36	0.66	3.86	0.76	2.06	0.30	1.99	0.29	21.0	127	0.97	0.97	0.88
	116—118	II	29.3	59.7	6.95	26.2	5.15	1.04	4.41	0.67	3.77	0.73	2.04	0.31	2.03	0.31	19.1	143	0.98	0.95	0.96
	153—155	II	27.7	56.2	6.61	25.1	4.94	1.01	4.30	0.65	3.72	0.73	1.99	0.30	1.99	0.29	19.0	135	0.98	0.95	0.94
	204—206	II	24.8	50.4	5.95	22.7	4.52	0.94	3.93	0.60	3.42	0.66	1.81	0.27	1.78	0.27	17.2	122	0.98	0.96	0.93
	232—234	II	26.3	52.9	6.28	23.9	4.79	1.00	4.27	0.66	3.75	0.74	2.00	0.30	1.97	0.29	19.4	129	0.97	0.96	0.90
	270—272	III	24.8	50.6	6.00	22.8	4.51	0.91	3.89	0.58	3.24	0.62	1.71	0.25	1.66	0.25	16.5	122	0.98	0.94	1.00
PLC-203	65—67	I	25.9	52.9	6.20	23.7	4.72	0.98	4.21	0.64	3.70	0.73	1.97	0.30	1.95	0.29	19.4	128	0.98	0.95	0.91
	109—111	I	26.0	52.6	6.17	23.6	4.68	0.97	4.08	0.62	3.51	0.68	1.87	0.28	1.82	0.27	18.1	127	0.98	0.96	0.97
	170—172	II	29.0	58.9	6.89	26.2	5.16	1.04	4.49	0.69	3.96	0.78	2.12	0.32	2.12	0.31	20.2	142	0.98	0.94	0.93
	218—220	II	27.9	57.1	6.66	25.4	5.01	1.03	4.32	0.65	3.70	0.72	1.97	0.30	1.98	0.29	18.7	137	0.99	0.96	0.96
	260—262	II	28.7	58.6	6.86	26.0	5.13	1.06	4.47	0.67	3.84	0.74	2.05	0.31	2.05	0.30	19.4	141	0.98	0.96	0.94
	278—280	II	27.1	55.3	6.48	24.6	4.89	1.01	4.33	0.66	3.84	0.75	2.05	0.30	2.03	0.30	19.5	134	0.98	0.96	0.90
Average		I	25.3	51.3	6.04	23.2	4.63	0.98	4.17	0.64	3.68	0.72	1.97	0.29	1.92	0.28	19.6	125	0.98	0.96	0.90
		II	26.5	53.8	6.33	24.1	4.79	0.99	4.22	0.64	3.70	0.72	1.98	0.30	1.97	0.29	19.2	130	0.98	0.96	0.91
		III	20.4	41.5	4.90	18.7	3.69	0.74	3.18	0.47	2.67	0.52	1.41	0.21	1.38	0.21	13.7	100	0.98	0.94	0.99

[a] $Ce/Ce^* = 2Ce_{UCCN}/(La_{UCCN} + Pr_{UCCN})$
[b] $Eu/Eu^* = 2Eu_{UCCN}/(Sm_{UCCN} + Gd_{UCCN})$

Table 4 Calculated enrichment factors (EFs) for some of the analyzed elements in the studied sediments.

Core ID	Horizon (cm)	Lithology Unit	EF_{Fe}	EF_{Mn}	EF_{Ag}	EF_{V}	EF_{Cr}	EF_{Co}	EF_{Ni}	EF_{Cu}	EF_{Zn}	EF_{Cd}	EF_{Ga}	EF_{Mo}	EF_{Sb}	EF_{Li}	EF_{Rb}	EF_{Cs}	EF_{Sr}	EF_{Ba}	EF_{Sn}	EF_{Sc}	EF_{Zr}	EF_{Hf}
CF-01	57—59	I	1.23	0.95	5.89	1.79	1.52	1.70	2.39	2.40	1.91	8.48	1.37	74.2	6.94	4.29	2.15	2.51	2.82	1.59	1.82	1.44	0.58	0.61
	93—95	II	1.24	0.89	5.02	1.73	1.54	1.55	2.36	2.74	1.91	8.41	1.39	72.2	4.55	4.38	2.12	2.50	1.05	1.62	1.76	1.51	0.57	0.59
	124—126	II	1.22	0.71	4.78	1.84	1.62	1.21	2.49	2.21	1.94	9.94	1.42	83.9	6.23	4.30	2.17	2.53	1.18	1.34	1.88	1.48	0.58	0.60
	155—157	II	1.23	0.84	5.57	2.17	1.80	1.63	3.53	3.19	2.26	14.0	1.57	74.6	5.76	4.73	2.37	2.85	1.34	1.35	2.06	1.69	0.56	0.61
	195—197	II	1.19	0.56	5.98	3.25	1.66	1.28	3.25	3.37	2.12	14.5	1.56	128	6.73	4.49	2.38	2.73	3.31	1.31	2.05	1.58	0.64	0.67
	218—220	III	1.21	0.73	4.10	1.63	1.50	1.09	1.69	1.73	1.79	5.84	1.39	8.5	5.57	3.71	1.99	2.10	1.72	1.22	1.99	1.29	0.58	0.63
CF-03	55—57	II	1.23	0.72	4.85	1.83	1.60	1.31	2.42	2.35	1.97	10.6	1.42	76.1	6.20	4.38	2.25	2.59	1.14	1.44	1.89	1.45	0.52	0.55
	104—106	II	1.18	0.57	4.94	1.92	1.58	1.25	2.60	2.58	1.98	12.3	1.42	88.7	6.03	4.42	2.18	2.62	1.11	1.78	1.78	1.46	0.59	0.62
	133—135	II	1.22	0.75	5.55	2.14	1.75	1.52	3.10	3.03	2.20	15.4	1.57	112	6.22	4.69	2.37	2.88	1.30	2.09	2.02	1.64	0.58	0.60
	170—172	II	1.15	0.62	5.23	2.43	1.56	1.10	2.63	2.69	1.83	13.6	1.38	61.9	6.48	3.85	2.02	2.19	1.67	1.20	1.89	1.36	0.64	0.68
	216—218	III	1.24	1.33	4.73	1.80	1.59	1.21	2.02	2.03	1.97	8.01	1.54	3.0	5.56	4.36	2.19	2.47	4.42	1.43	2.16	1.50	0.58	0.67
KL-01	165—167	II	1.22	0.86	5.20	1.94	1.70	1.37	2.72	2.68	2.04	10.8	1.48	92.3	4.99	4.46	2.34	2.78	1.03	1.24	1.98	1.52	0.52	0.55
	178—180	II	1.25	0.72	4.89	2.00	1.70	1.58	2.87	2.53	2.05	14.8	1.51	234	7.33	4.60	2.39	2.84	1.11	1.04	1.99	1.53	0.50	0.53
	200—202	II	1.20	0.52	5.03	2.40	1.67	1.33	3.15	2.71	2.08	12.7	1.51	176	7.92	4.50	2.33	2.79	3.79	1.05	2.00	1.54	0.56	0.59
	250—252	III	1.24	1.52	4.42	1.74	1.60	1.24	2.01	1.75	1.88	7.16	1.49	2.1	4.76	4.12	2.08	2.40	3.99	1.09	2.08	1.46	0.58	0.65
	294—296	III	1.20	1.10	4.99	1.80	1.63	1.19	2.03	1.73	1.96	7.06	1.56	1.9	4.10	4.26	2.18	2.40	3.17	1.12	2.22	1.50	0.65	0.71
KL-02	58—60	I	1.19	0.95	5.34	1.95	1.52	1.61	2.41	2.67	1.93	12.2	1.42	73.5	7.12	4.40	2.19	2.54	3.17	1.34	1.86	1.47	0.55	0.60
	86—88	I	1.22	0.96	6.06	1.91	1.57	1.68	2.62	2.66	2.00	9.91	1.44	57.9	5.04	4.45	2.25	2.62	3.23	1.57	1.94	1.50	0.55	0.59
	116—118	II	1.23	0.86	5.29	1.87	1.55	1.93	2.48	2.89	1.92	9.64	1.38	55.0	5.14	4.27	2.07	2.50	0.96	1.83	1.75	1.44	0.53	0.56
	153—155	II	1.21	0.69	5.01	1.85	1.57	1.29	2.36	2.29	1.89	9.66	1.42	61.6	4.68	4.32	2.21	2.58	1.15	1.70	1.85	1.44	0.55	0.59
	204—206	II	1.20	0.65	4.89	1.94	1.73	1.45	2.66	2.67	2.01	10.4	1.50	128	5.14	4.53	2.30	2.79	1.17	1.15	1.96	1.56	0.52	0.56
	232—234	II	1.27	0.73	4.62	2.19	1.71	1.77	3.27	2.50	2.03	11.6	1.50	166	7.59	4.39	2.31	2.74	1.14	0.96	2.00	1.53	0.56	0.59
	270—272	III	1.25	0.89	4.17	1.61	1.48	1.15	1.92	1.52	1.74	6.14	1.37	4.4	5.16	3.74	1.96	2.05	1.78	1.03	1.97	1.29	0.58	0.62
PLC-203	65—67	I	1.23	1.16	4.92	1.90	1.62	1.67	2.26	2.26	1.89	6.70	1.41	31.5	4.97	4.27	2.23	2.56	2.59	1.31	1.91	1.41	0.55	0.59
	109—111	I	1.21	0.85	4.90	1.89	1.51	1.53	2.11	2.05	1.85	5.94	1.35	27.8	5.35	4.18	2.11	2.47	1.89	1.39	1.83	1.36	0.48	0.52
	170—172	II	1.24	0.77	4.39	1.78	1.59	1.69	2.31	2.06	1.88	8.05	1.39	41.5	5.95	4.28	2.16	2.58	0.92	2.00	1.84	1.42	0.53	0.56
	218—220	II	1.28	0.80	4.38	1.75	1.70	1.73	2.41	1.90	2.00	6.93	1.43	44.7	4.21	4.30	2.26	2.73	0.91	1.01	1.89	1.43	0.52	0.56
	260—262	II	1.24	0.57	4.55	1.76	1.59	1.41	2.17	1.95	1.93	6.31	1.40	47.7	4.43	4.26	2.16	2.55	0.97	1.01	1.86	1.42	0.52	0.56
	278—280	II	1.29	0.96	4.81	1.84	1.75	1.67	2.56	2.28	2.10	7.97	1.49	80.0	6.34	4.50	2.28	2.74	1.02	1.11	2.01	1.54	0.58	0.62
Average		I	1.22	0.97	5.42	1.89	1.55	1.64	2.36	2.41	1.92	8.64	1.40	53.0	5.88	4.32	2.19	2.54	2.74	1.44	1.87	1.44	0.54	0.58
		II	1.23	0.73	5.00	2.03	1.65	1.48	2.70	2.56	2.01	10.9	1.46	96.1	5.89	4.40	2.25	2.66	1.38	1.38	1.92	1.50	0.56	0.59
		III	1.22	1.11	4.48	1.72	1.56	1.18	1.93	1.75	1.87	6.84	1.47	3.95	5.03	4.04	2.08	2.28	3.02	1.18	2.09	1.41	0.59	0.66

(*continued on next page*)

Table 4 (*continued*)

Core ID	Horizon (cm)	Lithology Unit	EF$_{Nb}$	EF$_{Ta}$	EF$_W$	EF$_{Tl}$	EF$_{Pb}$	EF$_{Th}$	EF$_U$	EF$_{La}$	EF$_{Ce}$	EF$_{Pr}$	EF$_{Nd}$	EF$_{Sm}$	EF$_{Eu}$	EF$_{Gd}$	EF$_{Tb}$	EF$_{Dy}$	EF$_{Ho}$	EF$_{Er}$	EF$_{Tm}$	EF$_{Yb}$	EF$_{Lu}$	EF$_Y$
CF-01	57—59	I	1.26	1.18	1.07	1.23	2.71	1.39	6.25	1.40	1.39	1.46	1.48	1.69	1.70	1.82	1.59	1.65	1.52	1.51	1.73	1.67	1.57	1.64
	93—95	II	1.20	1.12	0.98	1.11	1.85	1.33	3.62	1.31	1.30	1.35	1.34	1.53	1.50	1.58	1.38	1.43	1.32	1.31	1.49	1.51	1.45	1.37
	124—126	II	1.30	1.21	1.09	1.36	1.83	1.41	7.07	1.34	1.35	1.41	1.40	1.61	1.55	1.66	1.45	1.48	1.35	1.34	1.54	1.53	1.44	1.41
	155—157	II	1.32	1.25	1.24	1.36	2.05	1.52	9.04	1.45	1.44	1.51	1.54	1.78	1.77	1.95	1.71	1.80	1.68	1.69	1.97	1.93	1.90	1.88
	195—197	II	1.36	1.30	1.26	1.96	2.10	1.56	11.1	1.50	1.47	1.56	1.57	1.83	1.82	1.96	1.73	1.82	1.69	1.66	1.91	1.90	1.85	1.88
	218—220	III	1.41	1.35	1.15	1.09	1.69	1.44	2.21	1.48	1.49	1.56	1.56	1.77	1.68	1.79	1.55	1.57	1.44	1.41	1.57	1.59	1.52	1.50
CF-03	55—57	II	1.29	1.19	1.06	1.43	1.85	1.39	5.25	1.35	1.35	1.41	1.41	1.60	1.54	1.63	1.40	1.44	1.31	1.30	1.46	1.48	1.42	1.36
	104—106	II	1.22	1.13	1.02	1.29	1.85	1.37	7.49	1.30	1.29	1.35	1.34	1.52	1.47	1.56	1.37	1.43	1.31	1.32	1.50	1.53	1.45	1.38
	133—135	II	1.33	1.25	1.23	1.42	2.00	1.48	8.39	1.42	1.41	1.48	1.49	1.70	1.66	1.79	1.58	1.64	1.52	1.50	1.73	1.72	1.67	1.61
	170—172	II	1.38	1.32	1.16	1.89	1.76	1.38	6.82	1.42	1.39	1.49	1.50	1.72	1.70	1.82	1.58	1.63	1.50	1.50	1.72	1.69	1.60	1.63
	216—218	III	1.43	1.39	1.24	1.32	1.88	1.61	2.40	1.58	1.58	1.66	1.68	1.91	1.79	1.95	1.66	1.68	1.55	1.51	1.67	1.72	1.62	1.61
KL-01	165—167	II	1.30	1.23	1.13	1.24	1.94	1.45	7.39	1.38	1.39	1.45	1.45	1.65	1.62	1.70	1.48	1.52	1.39	1.37	1.57	1.55	1.47	1.44
	178—180	II	1.27	1.19	1.13	1.33	1.91	1.43	11.8	1.35	1.34	1.41	1.40	1.61	1.57	1.65	1.43	1.48	1.35	1.32	1.51	1.51	1.46	1.40
	200—202	II	1.29	1.21	1.16	1.46	1.98	1.49	14.0	1.42	1.41	1.49	1.50	1.72	1.69	1.83	1.58	1.63	1.48	1.46	1.66	1.65	1.61	1.59
	250—252	III	1.37	1.30	1.19	1.24	1.79	1.51	2.02	1.51	1.51	1.59	1.60	1.81	1.73	1.82	1.55	1.60	1.45	1.44	1.66	1.63	1.61	1.52
	294—296	III	14.8	1.44	1.25	1.24	1.88	1.63	2.37	1.72	1.72	1.79	1.79	2.01	1.85	2.02	1.70	1.70	1.53	1.50	1.76	1.71	1.62	1.60
KL-02	58—60	I	1.24	1.16	1.03	1.38	2.06	1.38	6.16	1.38	1.37	1.43	1.44	1.66	1.68	1.77	1.57	1.64	1.51	1.52	1.71	1.71	1.65	1.65
	86—88	I	1.30	1.21	1.08	1.43	2.77	1.45	4.74	1.47	1.46	1.53	1.55	1.80	1.80	1.94	1.68	1.77	1.63	1.60	1.78	1.77	1.67	1.78
	116—118	II	1.19	1.11	0.96	1.16	1.78	1.32	3.05	1.26	1.27	1.31	1.30	1.46	1.39	1.47	1.28	1.29	1.17	1.18	1.38	1.36	1.34	1.21
	153—155	II	1.28	1.20	1.04	1.47	1.86	1.39	4.00	1.32	1.32	1.37	1.37	1.55	1.49	1.58	1.37	1.41	1.30	1.28	1.47	1.47	1.38	1.33
	204—206	II	1.30	1.23	1.12	1.31	1.91	1.46	6.59	1.38	1.38	1.45	1.45	1.66	1.62	1.70	1.48	1.52	1.37	1.36	1.56	1.54	1.50	1.42
	232—234	II	1.31	1.23	1.19	1.27	1.95	1.47	6.41	1.39	1.37	1.44	1.45	1.66	1.63	1.74	1.54	1.57	1.46	1.42	1.63	1.61	1.53	1.51
	270—272	III	1.43	1.39	1.14	1.06	1.71	1.43	2.13	1.47	1.48	1.56	1.55	1.77	1.68	1.79	1.53	1.53	1.38	1.37	1.53	1.53	1.48	1.45
PLC-203	65—67	I	1.30	1.21	1.11	1.30	2.38	1.40	2.88	1.36	1.37	1.42	1.43	1.64	1.60	1.71	1.49	1.55	1.43	1.39	1.63	1.59	1.52	1.50
	109—111	I	1.24	1.15	1.02	1.31	2.08	1.32	2.20	1.28	1.28	1.33	1.34	1.52	1.48	1.56	1.35	1.38	1.25	1.24	1.43	1.39	1.33	1.32
	170—172	II	1.24	1.17	1.01	1.31	1.76	1.35	3.03	1.28	1.28	1.33	1.33	1.50	1.42	1.53	1.35	1.39	1.28	1.26	1.46	1.45	1.37	1.32
	218—220	II	1.29	1.21	1.06	1.29	1.87	1.38	2.78	1.31	1.32	1.36	1.37	1.55	1.49	1.57	1.35	1.38	1.26	1.24	1.45	1.44	1.36	1.29
	260—262	II	1.27	1.20	1.05	1.26	1.78	1.38	3.01	1.31	1.32	1.37	1.37	1.55	1.50	1.59	1.36	1.40	1.27	1.26	1.47	1.45	1.37	1.31
	278—280	II	1.36	1.28	1.19	1.28	1.91	1.48	3.83	1.39	1.40	1.46	1.45	1.66	1.61	1.73	1.50	1.57	1.44	1.42	1.59	1.62	1.54	1.48
Average		I	1.27	1.18	1.06	1.33	2.40	1.39	4.44	1.38	1.37	1.43	1.45	1.66	1.65	1.76	1.54	1.60	1.47	1.45	1.66	1.63	1.55	1.58
		II	1.29	1.21	1.11	1.38	1.89	1.42	6.56	1.36	1.36	1.42	1.42	1.62	1.58	1.69	1.47	1.52	1.39	1.38	1.58	1.57	1.51	1.46
		III	4.08	1.38	1.20	1.19	1.79	1.52	2.23	1.55	1.55	1.63	1.64	1.85	1.75	1.88	1.60	1.62	1.47	1.45	1.64	1.63	1.57	1.54
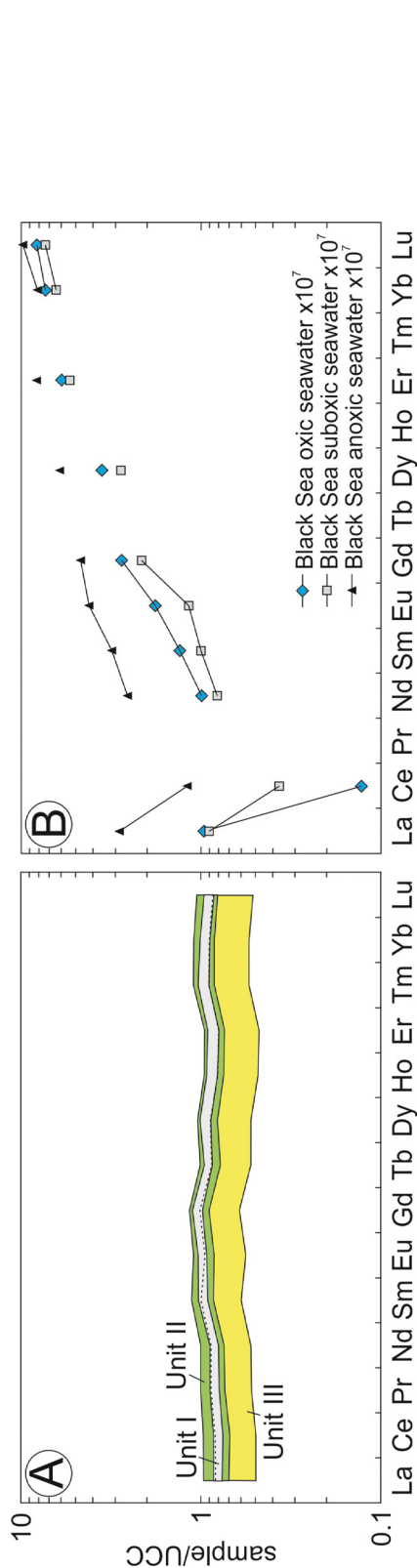
EF$_U$, EF$_{Cd}$ and EF$_{Sb}$ exhibit similar vertical profiles (Fig. 4) with strong enrichments at the base of Unit II, decrease in the enrichment towards Unit I and a following increase towards the upper part of Unit I. The general upward trend (from Unit III to Unit I) in the enrichment factors of Sn, Th, La (representative for the light REE), Lu (representative for the heavy REE), Nb and Ta is a decrease through Units III and II, and a sharp increase in Unit I (Fig. 4). These elements are enriched (relative to the UCC) in all the three stratigraphic units (Fig. 4). Vertical profiles of the enrichment factors of Pb and Ag are similar to upward increases and maxima in Unit I (Fig. 4). The EF$_{Zr}$ and EF$_{Hf}$ co-vary, but both elements are depleted (relative to the UCC) in all the three stratigraphic units, particularly in the sapropel layer (Fig. 4).

4.2. Sr-Nd-Pb-isotope composition of the terrigenous component of the sediments

The Sr-Nd-Pb-isotope composition of the terrigenous component of the studied sediments (Table 5) is relatively uniform and there are only minor differences between samples from different sites and between those from different stratigraphic units. Strontium isotope composition (^{87}Sr/^{86}Sr) of this component is generally quite radiogenic compared to the Black Sea water signature (^{87}Sr/^{86}Sr$_{Last\ Glacial\ Maximum} = 0.70865-0.70875$, ^{87}Sr/^{86}Sr$_{modern} = 0.709133$; Major et al., 2006) and has a total range from ~0.7196 to 0.7224. Both the lowest and highest values were measured in the sapropel samples: from cores CF-03 and PLC-203, respectively (Table 5). Furthermore, there is a general tendency of ^{87}Sr/^{86}Sr variation across the boundaries between the stratigraphic units, but there is no simple relationship between the Sr isotope ratios and Sr concentration as exemplified by data from core Kl-02 (Fig. 5). The overall Nd isotope pattern is similar to that observed for the Sr isotope system: εNd values are relatively homogeneous and range from -8.0 to -10.2, with one lower value (-12.5) in core PLC-203 (Table 5). Although the variations are overall small, ^{206}Pb/^{204}Pb decreases upward (from Unit III to Unit I) along each sediment core (Table 5; Fig. 5), and this vertical distribution is also observed for the Nd isotopes for the same profile (Fig. 5). However, the other two Pb isotope ratios show similar values for all samples irrespective of their lithology although data from core PLC-203 generally are somewhat more radiogenic (Table 5). The binary relations of Sr-Pb, Sr-Nd and Nd-Pb isotopes (not shown) do not indicate any obvious linear trends related to stratigraphic position within a core.

5. Discussion

5.1. Element enrichment in organic-rich sediments

5.1.1. Iron

The Fe enrichment observed in the Black Sea organic-rich sediments (Units II and I) is inferred to be of neither diagenetic origin (Eckert et al., 2013; Lyons and Severmann, 2006) nor is it a result of preferential physical transport of reactive Fe-rich detrital component to the deep basin

Figure 3 UCC-normalized (Rudnick and Gao, 2003) REE distribution patterns of: (A) studied Black Sea Quaternary sediments from Unit I (coccolith ooze), Unit II (sapropel) and Unit III (terrigenous mud); (B) oxic (50 m water depth), suboxic (100 m water depth) and anoxic (2185 m water depth) seawater from Black Sea (German et al., 1991).
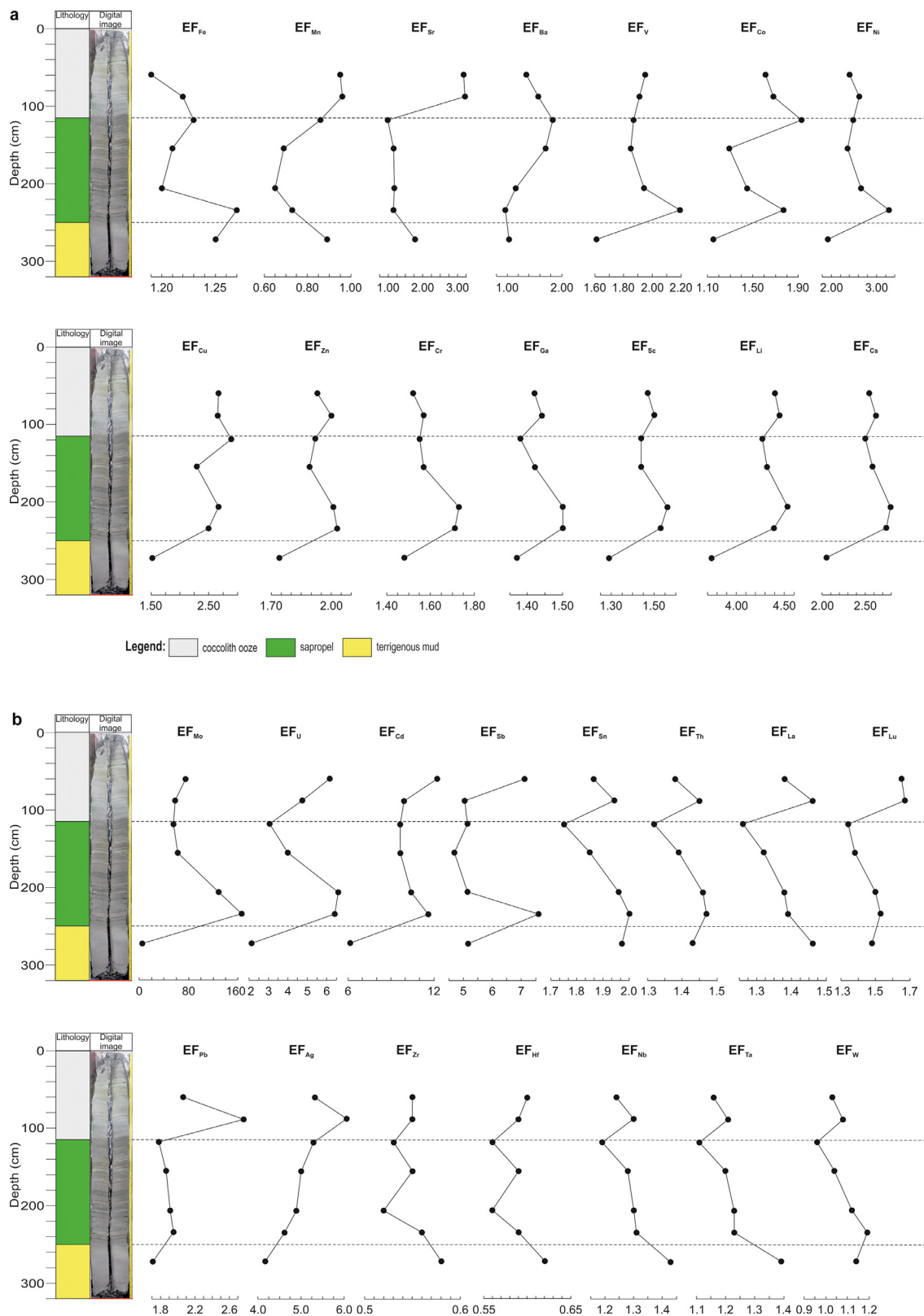
Figure 4   Vertical profiles of enrichment factors (EFs) of some elements along the sediment core KL-02.

Table 5 Isotope composition of the terrigenous component of the studied sediments.

Core ID	Horizon (cm)	Lithology Unit	$^{87}Sr/^{86}Sr$	$\pm2\sigma_m$	$^{143}Nd/^{144}Nd$	$\pm2\sigma_m$	$\varepsilon_{Nd(0)}$	$^{206}Pb/^{204}Pb$	$^{207}Pb/^{204}Pb$	$^{208}Pb/^{204}Pb$
CF-03	55—57	II	0.720946	9	0.512113	14	-10.24	18.893	15.669	38.918
	104—106	II	0.719618	10	0.512157	3	-9.38	18.877	15.659	38.895
	133—135	II	0.720269	8	0.512163	3	-9.27	18.875	15.667	38.895
	170—172	II	0.719619	8	0.512175	5	-9.03	18.906	15.671	38.871
	216—218	III	0.721602	9	0.512168	5	-9.17	19.008	15.682	38.927
KL-01	165—167	II	0.721683	10	0.512194	3	-8.66	18.886	15.669	38.908
	178—180	II	0.722007	9	0.512213	6	-8.29	18.874	15.670	38.907
	200—202	II	0.720938	6	0.512147	5	-9.58	18.914	15.669	38.923
	250—252	III	0.722410	7	0.512230	19	-7.96	19.010	15.683	38.947
	294—296	III	0.721951	8	0.512129	10	-9.93	19.120	15.697	39.177
KL-02[a]	58—60	I	0.721513	9	0.512171	4	-9.11	18.814	15.666	38.901
	86—88	I	0.721241	9	0.512169	3	-9.15	18.801	15.661	38.887
	116—118	II	0.720371	8	0.512175	4	-9.03	18.834	15.663	38.914
	153—155	II	0.721124	12	0.512162	4	-9.29	18.838	15.664	38.893
	204-206	II	0.722097	9	0.512162	3	-9.29	18.838	15.666	38.909
	232—234	II	0.721857	6	0.512168	3	-9.17	18.844	15.666	38.895
	270—272	III	0.721258	9	0.512137	5	-9.77	18.892	15.675	38.985
PLC-203	65—67	I	0.722630	13	0.512168	27	-9.17	18.907	15.680	39.053
	109—111	I	0.722593	8	0.512137	6	-9.77	18.977	15.692	39.062
	170—172	II	0.722119	8	0.512164	18	-9.25	18.978	15.691	39.054
	218—220	II	0.722543	9	0.511995	8	-12.54	18.981	15.691	39.062
	260—262	II	0.722696	8	0.512126	41	-9.99	19.018	15.696	39.082
	278—280	II	0.722809	8	0.512135	6	-9.81	18.981	15.694	39.045
BCR-2[b]			-		0.512620	7		18.751	15.624	38.719
BCR-2[b]			0.705017	6	0.512663	10		18.777	15.616	38.755

[a] Pb isotope data were partly obtained by a Micromass Isoprobe, the others by a Nu Plasma II instrument. The $^{87}Sr/^{86}Sr$ values of the samples were corrected to $^{87}Sr/^{86}Sr = 0.710245$ for the NIST SRM-987 Sr standard. No external corrections were required for the Nd runs.

[b] Unleached data.
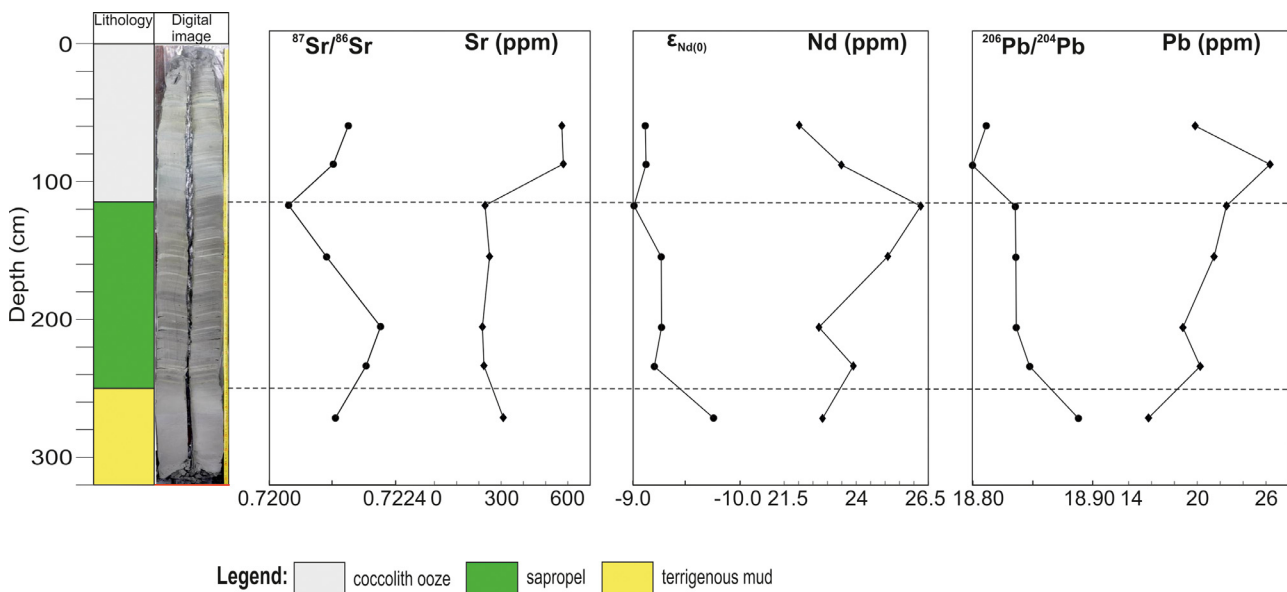
Figure 5 Vertical profiles of Sr, Nd, Pb isotope ratios and elemental concentrations along the sediment core KL-02.

(Lyons and Severmann, 2006). The reactive Fe enrichment of these sediments has been recognized (Anderson and Raiswell, 2004; Canfield et al., 1996; Lyons and Severmann, 2006; Raiswell and Anderson, 2005) as a uniquely euxinic phenomenon. Dissolved Fe supply to the euxinic pool has been attributed to the operation of a benthic Fe redox shuttle. According to this model (Lyons and Severmann, 2006), in oxic to suboxic sediments (now at the Black Sea shelf) with organic matter content high enough to produce anoxia, but not enough to create H_2S production by SO_4^{2-} reduction, the deposited Fe-oxyhydroxides are dissolved in the sediment. Produced Fe^{2+} is mobile in the anoxic pore fluids and diffuses into the bottom seawater. Then it can be transported into the euxinic deep waters of the basin where it reacts with dissolved H_2S and forms sulfides that settle down on the seafloor (Lyons and Severmann, 2006). This process strips almost completely the dissolved Fe out of the euxinic deep seawater.

This general model was further developed by Eckert et al. (2013) in their attempt to explain the variations of Fe enrichment in the Holocene Black Sea sediments. A key point of this model, based on the evolution of euxinia in the Black Sea, is the temporal fluctuation of the chemocline which is the primary contributor of dissolved Fe to the enxinic pool. In our endeavor to explain the observed vertical distribution of the Fe enrichment in the studied sediments (Fig. 4) we employ this model (Eckert et al., 2013) with two new assumptions: (1) the establishment of euxinia in the deep Black Sea started with onset of suboxia that gradually evolved to euxinia; (2) the chemocline, developed during the evolution of the deep water from oxic to euxinic, has not undergone substantial fluctuations during its rise up to the shelf.

The last ingression of Mediterranean seawater into the Black Sea through the narrow and shallow Bosporus Strait started at ~9 ka BP (Bahr et al., 2005, 2008; Soulet et al., 2011). The inflow of saline marine waters marks the last transition of the Black Sea from oxic lacustrine to the euxinic marine basin (Fig. 6a). The Black Sea deep waters evolved from oxic to suboxic as a result of oxygen depletion due to saline stratification of the water column, incurred reduced vertical ventilation and oxygen consumption due to respiration of organic matter (Murray et al., 1991). The sediment at vast areas of the abyssal plain and the lower continental slope produced high Fe^{2+} flux to the bottom water as a result of the benthic Fe redox shuttle mechanism (Lyons and Severmann, 2006) (Fig. 6a). Progressively increasing concentration of the dissolved H_2S due to microbial SO_4^{2-} reduction increased the amount of precipitated dissolved Fe^{2+} as Fe-sulfides recorded as a peak in the Fe enrichment at the base of Unit II (Fig. 6b). Further development of the euxinia resulted in an increase of the volume of the deep euxinic waters and a rise of the chemocline (suboxic zone) formed between euxinic (deep) and oxic (surface) waters upward the continental slope. Seafloor overlaid by euxinic waters did not produce dissolved Fe anymore because the released Fe^{2+} within the sediment was sulfidized *in situ* by dissolved H_2S. Thus, the narrow band where the chemocline impinged the continental slope became the major source of Fe^{2+} to the euxinic pool. Since the magnitude of released Fe^{2+} flux is a function of the source area (Lyons and Severmann, 2006) the Fe^{2+} supply and consequently Fe-sulfide

deposition during this stage was reduced. This is recorded as a decrease of the EF_{Fe} in the middle part of Unit II (Fig. 6c). We interpret the next maximum of the Fe enrichment at the upper part of Unit II (Fig. 4) as a result of a further rise of the chemocline and its impingement on the continental shelf: i.e., a further increase in the source area and related increase in the dissolved Fe^{2+} flux, and consequent Fe-sulfide burial in the deep basin (Fig. 6d). According to previous estimates (Eckert et al., 2013) the rising chemocline reached the shelf at ~5.3 ka BP. The second maximum of the EF_{Fe} in our cores is before the transition between Units II and I (Fig. 4) dated at ~3 ka BP (Kwiecien et al., 2008). However, the increase of the EF_{Fe} begins earlier (Fig. 4) which may be interpreted as the beginning of the chemocline incursion into the shelf (Fig. 6d). It may roughly be estimated at ~5 ka BP, which is in line with the previous studies (Eckert et al., 2013). The following decrease in the Fe enrichment towards the middle of Unit I (Fig. 4) may be explained by an exhaustion of the source shelf sediments in Fe and a related decrease in the dissolved Fe flux to the euxinic pool. We may speculate that this situation has not evolved dramatically up to now when the chemocline (span from ~50 to 100 m water depth; Murray et al., 1989) impinges at the shelf (shelf edge at ~150 m water depth; Degens and Ross, 1974) (Fig. 1c,d).

5.1.2. Manganese

A benthic redox shuttle similar to that for Fe is supposed to operate for Mn as well (Lyons and Severmann, 2006). However, the enrichment profile of Mn differs from that of Fe (Fig. 4), which means that the mechanisms of enrichment/depletion of reactive Mn and Fe in the studied euxinic sediments differ from each other. The key details are that the Mn is, in general, depleted in these euxinic sediments (Units II and I; Table 4, Fig. 4) and it is most depleted in the sapropel layer (Unit II). This general Mn depletion (against UCC) is in accord with a previous suggestion (Konovalov et al., 2007) that Mn is not accumulated in sediments of the Black Sea anoxic zone where all our cores are located (Fig. 1c,d; Table 1).

The euxinic sediments (Units I and II) of the Black Sea sedimentary cover have a high content of organic matter (Calvert, 1990; Calvert et al., 1987; Degens and Ross, 1972; Glenn and Arthur, 1985; Ross et al., 1970) (Fig. 2). The organic matter degradation is the principal process that drives the dissolution and reprecipitation of a number of mineral phases within the sediment and provides both sources and sinks (respectively) of global importance to the geochemical mass balance of trace metals in the ocean (Emerson and Hedges, 2003). Therefore, a diagenetic (caused by organic matter degradation) redistribution of the redox-sensitive elements across the organic-rich Units I and II may be anticipated.

Manganese is a redox-sensitive element and therefore when interpreting the vertical profile of EF_{Mn} (Fig. 4) we considered the vertical distribution of Mn^{2+} concentrations in the Black Sea sediment pore fluids (Konovalov et al., 2007). The $[Mn^{2+}]_{pore\ fluid}$ profile shows an upward Mn^{2+} flux (Konovalov et al., 2007) indicating a diagenetic Mn_{solid} dissolution and Mn^{2+} diffusion towards the bottom seawater. The similarity of this profile to that of the EF_{Mn} we observed in the studied sediments (Fig. 4) implies that the vertical distribution of the reactive Mn in these sediments is primar-
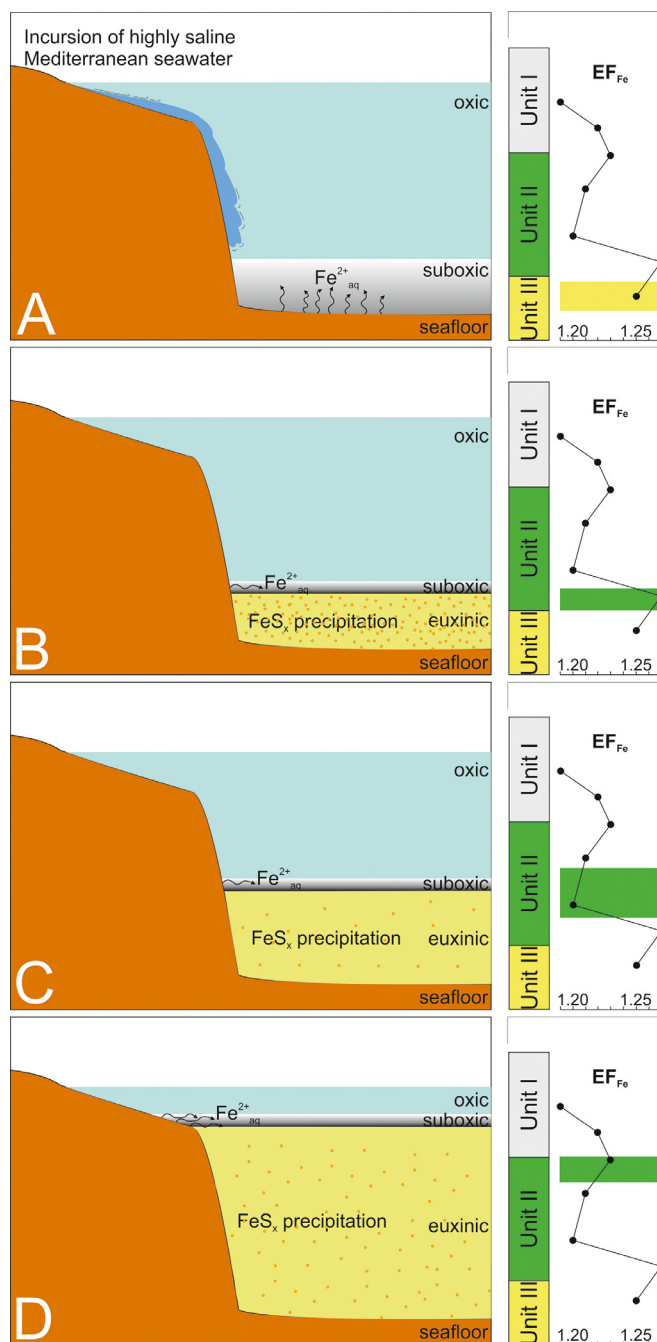
Figure 6 Schematic representation of Fe enrichment (as EF_{Fe}) in the Holocene sediments of the western Black Sea as a result of euxinia development and migration of suboxic layer (chemocline) upward the continental slope. (a) As a result of the incursion of Mediterranean saline waters in the Black Sea at ∼9 ka BP the Black Sea deep waters evolved from oxic to suboxic. The sediment overlain by the suboxic waters produced high Fe^{2+}_{aq} flux to the bottom water as a result of the benthic Fe redox shuttle mechanism. The small fraction of the dissolved Fe^{2+}_{aq} was reprecipitated as sulfides due to reaction with H_2S, which started appearing as a result of microbial SO_4^{2-} reduction. (b) Deep suboxic waters evolved to euxinic with the progressive increase of H_2S concentration. This led to a quantitative removal of the accumulated Fe^{2+}_{aq} as Fe-sulfides that settled at the seafloor. Fe(-sulfide) deposition was recorded as a peak in the Fe enrichment at the base of Unit II. A thin suboxic layer developed as a transition zone (chemocline) between the deep euxinic waters and oxic water above them. (c) Development of the euxinia resulted in an increase of the volume of the deep euxinic waters and a rise of the suboxic layer upward the continental slope. Sediment overlain by euxinic waters did not produce Fe^{2+}_{aq}. The narrow band where the suboxic layer impinged the continental slope became the major source of Fe^{2+}_{aq} to the euxinic pool. Reduced Fe^{2+}_{aq} supply led to a reduced Fe-sulfide deposition recorded as a decrease of the EF_{Fe} in the middle part of Unit II. (d) Further increase of the volume of euxinic deep pool led to a rise of the chemocline (suboxic layer) and its impingement on the continental shelf. This resulted in an increase in the source area, related increase in the Fe^{2+}_{aq} flux to the deep euxinic basin, and consequent high Fe-sulfide precipitation. This is recorded as a second maximum of the Fe enrichment at the upper part of Unit II. (For more explanations see the text.)

ily controlled by diagenetic processes: dissolution in Unit II, diffusion to and reprecipitation in Unit I (Fig. 4). While we agree with the previous observations that Mn is not accumulated in sediments of the Black Sea anoxic zone (Konovalov et al., 2007) ($EF_{Mn} < 1$; Table 4) the maximum of EF_{Mn} in Unit I (Fig. 4) suggests for some Mn_{solid} accumulation there. If we suppose the diagenetic dissolution of Mn_{solid} in Unit II and upward Mn diffusion, the Mn reprecipitation in Unit I has to be controlled by the solubility of Mn solid phases. Pore fluids in the Black Sea anoxic sediments are anoxic (Konovalov et al., 2007) and we cannot expect Mn-oxide precipitation in the Unit I. Konovalov et al. (2007) measured high flux of dissolved sulfide from Unit I to the bottom seawater and concluded that the sulfide source is in Unit II from where it diffuses upward. We may speculate that Mn dissolved from Unit II diffuses upward along with sulfide and its precipitation in Unit I is controlled by the solubility of Mn-sulfides.

5.1.3. Barium

A major part of Ba in marine sediments was found to be in the biogenic barite, $BaSO_4$ (Goldberg and Arrhenius, 1958). Barite is highly refractory under oxic conditions, but under anoxic conditions, it dissolves and may further re-precipitate (Henkel et al., 2012). Previous studies suggest that a significant fraction of non-detrital Ba deposited at the seafloor is recycled during diagenesis within the sediment and may even be released back to the seawater (McManus et al., 1994, 1998). Diagenetic reactions related to the organic matter decomposition play a certain role in the dissolution and diffusive flux of Ba back into the ocean (Monnin et al., 2001). Thus, the Ba cycling in the sediment is primarily controlled by the content of organic matter. In the presence of organic matter microbially-mediated reduction of seawater-derived SO_4^{2-} consumes it (SO_4^{2-}) from the pore fluids progressively downward. When the SO_4^{2-} is totally consumed, methanogenesis takes over as the dominant process of organic matter decomposition and the CH_4 content increases further downward the sediment (Henkel et al., 2012). The zone in the sediment where the SO_4^{2-} disappears and CH_4 appears in the pore fluids is termed sulfate-methane transition (SMT). The SMT is an important redox boundary with respect to the Ba cycle. Above it, the $BaSO_4$ is stable because of the presence of SO_4^{2-}. Below it, the absence of SO_4^{2-} results in $BaSO_4$ dissolution and diffusion of Ba^{2+} towards the above sulfate-containing zone where it may re-precipitate as $BaSO_4$. The high-resolution studies of pore fluids and sediments from the NW Black Sea (Henkel et al., 2012) revealed that the SMT in this area is located within the lower part of Unit II. Solid Ba_{xs} (Ba enrichment) was documented to gradually decrease upward Unit III and reaches minimum values below or slightly above the Unit III/Unit II boundary (Henkel et al., 2012). Diagenetic Ba enrichment was found at and slightly above the SMT (Henkel et al., 2012). Ba_{xs} is high in the upper part of Unit II and decreases upward in Unit I (Henkel et al., 2012).

Ba enrichment profile (expressed as EF_{Ba}) recorded in our sediments (Fig. 4) is similar to that (expressed as Ba_{xs}) described in the sediments cored in the NW Black Sea (Figs 2 and 3 in Henkel et al., 2012). Ba depletion in the upper part of Unit III and lower part of Unit II, and Ba enrichment in the upper part of Unit II (Fig. 4) suggests that the SMT

in the studied area of the western deep Black Sea (Fig. 1a,b) is localized within the middle part of Unit II. This interpretation is supported by the location of the maximum of $C_{org.}$ concentration in the lower part of Unit II (Fig. 2). The EF_{Ba} peak just at the Unit II/Unit I boundary (Fig. 4) likely represents the current authigenic $BaSO_4$ front.

5.1.4. Copper, Co, Ni, Zn, Cr, W, Mo, V, Cd and Sb

In the presence of free H_2S in the seawater column and in the sediment pore fluids the excess reactive Fe precipitates as Fe-sulfide. Fe-sulfides found in the Black Sea sediments include pyrite (FeS_2) and Fe-monosulfides (disordered FeS, mackinawite (FeS_{1-x}), and greigite (Fe_3S_4)) (Franke et al., 2009). It has been shown that at high H_2S concentrations the Fe-monosulfides transform into pyrite in euxinic marine sediments (Hurtgen et al., 1999). Thus, pyrite appears to be one of the major authigenic minerals found to form in anoxic-euxinic sediments (Berner, 1981). Pyrite can be an important sink for a range of trace elements (Boulègue et al., 1982). Investigations of trace element incorporation in authigenic pyrite in a variety of redox environments (Huerta-Diaz and Morse, 1992) revealed that co-precipitation is the mechanism of incorporation of these elements into pyrite. The magnitude of this incorporation is a function of both the amount of precipitated pyrite and the concentrations of trace elements in the reactive fluid (Huerta-Diaz and Morse, 1992). Thus, the authigenic pyrite appears to be an important sink for Mo, moderately important for Co, Cu and Ni, and of less importance for Cr, Zn and Cd. The highest values of the degree of trace metal pyritization were found in anoxic-euxinic environments (Huerta-Diaz and Morse, 1992).

The co-variation of Cu and Co enrichments with that of Fe along the entire cored sediments, and the co-variation of Ni, Zn, Cr, W, Mo, V, Cd and Sb enrichments with that of Fe in the upper Unit III and lower Unit II (Fig. 4) suggest that these trace elements might have been incorporated into authigenic Fe-sulfides (e.g., pyrite) in the respective sediments. Co-precipitation may have been a possible mechanism of their incorporation in the Fe-sulfides. Nickel, Zn, Cr, W, Mo, V, Cd and Sb decouple from Fe in the Unit I (Fig. 4) and this implies that the major part of these elements in this sediment layer may not be co-precipitated with Fe within Fe-sulfides. This series of elements can be divided in two groups according to their vertical distribution in Unit I: Ni, Zn, Cr, W, and Mo, V, Cd, Sb. The enrichments of Ni, Zn, Cr and W co-vary with that of Mn and it is possible that like Mn these elements were subjected to diagenetic redistribution in Unit I: dissolution in the upper part of Unit II, diffusion to and reprecipitation in Unit I (Fig. 4).

The enrichments of Mo, V, Cd and Sb co-vary in the upper part of Unit II and Unit I (Fig. 4) and this implies that they might have had a similar mechanism of precipitation. Although the precise mechanisms of Mo sequestration from euxinic waters and its transfer to sediment are debatable (Little et al., 2015), the strong correlation of Mo enrichment with that of Fe in the upper Unit III and lower Unit II (Fig. 4) suggests that Fe-sulfides played a major role as host for Mo (as well as for V, Cd and Sb) at the onset of Holocene marine stage of the Black Sea evolution. The

strong decrease in EF_{Mo} towards upper Unit II and Unit I (Fig. 4) can be explained by the "basin reservoir effect" (Algeo and Lyons, 2006): Mo enrichment has decreased in the increasingly stagnant Black Sea water body due to Mo removal to the sediment without adequate resupply by deep water renewal. In a similar way the "basin reservoir effect" seems to be responsible for the vertical distribution of the V, Cd and Sb enrichments in Unit I (Fig. 4). Weak enrichments in the topmost studied sample (Fig. 4) may be due to a recent increase in the element supply.

5.1.5. Uranium

Uranium is enriched under anoxic conditions (Morford and Emerson, 1999) and it is not surprising that the Holocene organic-rich sediments in the Black Sea are about one order of magnitude richer in U than the average marine sediment (Degens et al., 1977). Spatial (basin-wide) and temporal (along the sediment cores) variations of the U enrichment in the Black Sea sediments (Barnes and Cochran, 1991) imply that there may be several controls on this enrichment. Degens et al. (1977) provided evidence that the planktonic organic matter is the principal carrier of enhanced content of U and concluded that this was the reason for U enrichment in the coccolith ooze (Unit I). However, the C_{org} concentrations across the studied coccolith ooze layer (Unit I) decrease upwards (Fig. 2) whereas the EF_U increases (Fig. 4). This rules out the possibility that the planktonic organic matter is responsible for the U enrichment in Unit I. Studies of Barnes and Cochran (1991) showed that authigenic U (excess over the lithogenic background) is supplied to the uppermost sediment (<38 cm) via diffusion from the bottom seawater. Although we are not aware of any high-resolution studies of the pore fluid U distribution across the coccolith ooze layer (Unit I) down to the Unit I/Unit II boundary we may speculate that the U enrichment in the upper Unit I (Fig. 4) is a result of the influence of the bottom seawater U flux. Low EF_U in the terrigenous mud (Unit III; Fig. 4) is likely due to both low organic matter content in it (Fig. 2; see also Degens et al., 1977) and oxic conditions in the basin (lacustrine stage) during the deposition of this layer in which U is highly mobile. Explanation of the U enrichment distribution across Unit II is challenging. High U enrichment in the lower Unit II (Fig. 4) coincides with a peak of organic matter content (Fig. 2; see also Degens et al., 1977). However, this organic matter was found to be mostly land-derived and not rich in U (Degens et al., 1977). EF_U maximum right after the transition from oxic to euxinic conditions in the deep Black Sea (above the boundary Unit III/Unit II) (Fig. 4) can be explained by continuous reduction of U dissolved in oxic lake water and its quantitative (complete) removal to the sediment in euxinic brackish-marine water. The upward decrease of the EF_U towards the Unit II/Unit I boundary (Fig. 4) is interpreted as a "basin reservoir effect": U removal without resupply by deep water renewal. Thus, the two U enrichments, at the base of Unit II and in Unit I (Fig. 4), likely have different genesis and neither of them is directly related to the C_{org} content. We hypothesize that the enrichment at the base of Unit II is at the expense of the U inventory of the deepwater pool and is a result of inorganic reduction of U in euxinic environment. The enrichment in Unit I is supposed to be a result of the bottom seawater U influx.

5.1.6. Zirconium, Hf, Nb, Ta and Li, Rb, Cs, Ga, Sc

The high field strength elements Zr, Hf, Nb and Ta are closely linked to the detrital component in marine sediments and their concentrations are primarily controlled by the proportion of detrital and biogenic phases (Plank and Langmuir, 1998). Therefore, the depletion of Zr and Hf in the organic-rich Units II and I (Fig. 4) obviously reflects a significant dilution of the detrital component with biogenic component (C_{org} and $CaCO_3$; Fig. 2). Similarly, the weak enrichment of Nb and Ta over the UCC abundance in Unit III (Fig. 4) suggests low biogenic dilution of the detrital background. According to previous estimates (Calvert and Karlin, 1998) the accumulation rate of lithogenic matter in Unit II is lower than that in Unit I, which accounts for the higher depletion of Zr and Hf in Unit II (Fig. 4). In addition to the dilution effect of the biogenic component on the detrital component, the values of the enrichment factors of these elements are affected by (probably) the slight difference between the chemistry of the local detrital component and that of the UCC (grand average values).

Enrichments of Li, Rb, Cs, Ga and Sc co-vary with those of Ni, Zn, Cr and W (Fig. 4), but it is challenging to suppose that these elements may have been subjected to diagenetic redistribution in Units II and I like Ni, Zn, Cr and W (e.g., 5.1.4). Lithium, Rb, Cs, Ga and Sc are considered to be mostly detrital in the marine sediments (Goldberg, 1954; 1961), but their EFs do not show clear correlation with those of the other detrital elements (e.g., Zr, Hf, Nb and Ta) (Fig. 4). The only assumption we can make is that the values of the EF of these elements are affected by the difference between the chemistry of their carrier (local detrital component) and that of the UCC.

5.1.7. Rare earth elements, Sn and Th

REE distribution patterns of the studied sediments (Fig. 3) indicate that their REE composition is principally controlled by the lithogenic matter. No detectable influence of seawater-derived components (e.g., organic matter, biogenic $CaCO_3$) (Fig. 3b) is observed. Thus, the weak REE enrichments estimated in all the three stratigraphic units (Table 4; Fig. 4) must be controlled by the lithogenic matter. A possible mechanism of enrichment of the lithogenic matter in REE over the UCC values is the adsorption on clay minerals. A large body of evidence demonstrates that the REE adsorption on clay minerals is of great importance in the sedimentary geochemistry of the REE (Aagaard, 1974; Bruque et al., 1980; Takahashi et al., 2004; Tertre et al., 2005; Wan and Liu, 2005). The lowest REE enrichment in Unit II (Fig. 4) likely reflects the lowest accumulation rate of the lithogenic matter in this sediment layer (Calvert and Karlin, 1998).

The inverse correlation between ΣREE and SiO_{2det}/Al_2O_3 ratio (Tables 2, 3) is in accord with the suggestion that SiO_{2det}/Al_2O_3 ratio of the studied sediments is higher than that of the UCC due to high quartz content in the former (see 5.1.9). Quartz is known to contain very low amounts of REE (McLennan, 1989). Hence, the high SiO_{2det}/Al_2O_3 ratio means high quartz content, which in turn implies low ΣREE (dilution effect of low-REE quartz). Therefore, SiO_{2det}/Al_2O_3 and ΣREE correlate inversely.

The enrichments of Sn and Th co-vary with those of the REE (Fig. 4) and, similarly, are interpreted to be related to adsorption on clay minerals.

5.1.8. Calcium and Sr

In marine sediments Sr is mostly held in the $CaCO_3$ crystal lattice and therefore, its variations are controlled by the relative proportions of $CaCO_3$, clays and biogenic opal (Goldberg and Arrhenius, 1958; Plank and Langmuir, 1998). Perfect co-variation of $CaCO_3$ and Sr in the studied sediments (Figs 2, 4) suggests that the biogenic $CaCO_3$ is the main carrier of Sr. Strontium depletion in Unit II and enrichment in Units III and I confirm the well-known decrease and increase, respectively, of the $CaCO_3$ content across the succession of these sediment units (Ross and Degens, 1974).

5.1.9. Silicon

The observed excess of detrital SiO_2 in the studied sediments over the UCC [$(SiO_{2det}/Al_2O_3)_{samples} = 4.5-7.8$, $(SiO_2/Al_2O_3)_{UCC} = 4.3$] (see *4.1.1*) can be explained with local enrichment in SiO_2 of the detrital material supplied to the western Black Sea. We may speculate that this detrital material might have been enriched in quartz (SiO_2). The SiO_2/Al_2O_3 ratio is considered as an indicator of mineralogical and textural maturity of the sediments (Pettijohn et al., 1972). The higher the ratio the greater the maturity, which in turn implies the sediments have undergone a larger sedimentary cycle. We infer that the major part of the detrital component in the western Black Sea sediments might have been delivered from a distal source that has resulted in detrital material refinement and its slight enrichment in quartz.

SiO_{2am} maximum in the sapropel layer (Unit II) and its covariation with C_{org} (Fig. 2; Table 2) confirms the biogenic origin of both components (Pilskaln and Pike, 2001). As the studied sediments are located at the continental slope (Table 1; Fig. 1b—d) there is a probability that the biogenic silica (SiO_{2am}) and C_{org} in them may have not originated from the pelagic sedimentation, but may have come from the continental shelf through downward transport along the slope (e.g., Ragueneau et al., 2009). In order to investigate this potential source of SiO_{2am} and C_{org} in the sediments, we calculated the Si_{am}/C_{org} molar ratio in our samples (Table 2). This ratio (0.09 in Unit I, 0.08 in Unit II and 0.12 in Unit III, in average) is lower than that of the continental shelf sediments (~ 0.6) and open ocean siliceous oozes (20—60) (DeMaster et al., 1991), and comparable to that of most living marine diatoms grown under replete nutrient conditions: 0.13 (Brzezinski, 1985). It suggests that the SiO_{2am} and C_{org} in the studied sediments have not originated at the shelf and transported afterward to the continental slope, but are likely a result of pelagic sedimentation. It also implies that there has been no preferential preservation of Si_{am} relative to C_{org} after burial (usually observed, with Si_{am}/C_{org} ratios increasing typically up to 0.5—1 in the Atlantic deep-sea sediments and up to 10 in equatorial Pacific sediments; Ragueneau et al., 2002) and both biogenic components have remarkably been preserved likely due to the anoxic conditions in the basin. Thus, Si_{am}/C_{org} molar ratio appears to be a good indicator for C_{org} preservation.

5.2. Sr-Nd-Pb isotope constraints on the source and type of terrigenous component

Sr-Nd-Pb isotope data, inferred to represent the isotope composition of the terrigenous component of the studied sediments in the western Black Sea, show quite homogenous values (Table 5). Although some intra-core isotope variations exist, particularly noted for the Nd component in sample PLC-203 (260—262), neither of the sediment cores have isotopic values that are clearly distinct from any of the others. These minor isotopic differences are not unexpected given that the studied sites occupy a small geographic area, and they are in agreement with the recognized uniform depositional environment within the entire deep Black Sea during the Late Quaternary (Ross et al., 1970). Yet, this isotope homogeneity is quite remarkable considering that the studied sediments were deposited during variable climatic conditions, implying variations in both erosion rates and wind regimes over the sediment supplying provenances. Fluctuations in the riverine and aeolian sediment supplies are known to cause variations in the isotope composition of sapropel-containing sedimentary successions (e.g., Eastern Mediterranean Sea; Weldeab et al., 2002).

Basically, the terrigenous component of marine sediments can be supplied in two major ways: riverine (river flux) and aeolian (wind-blown flux). Five potential sources of this component might be considered given the location of the studied sediment cores (Fig. 1a,b): (A) material supplied to the NW Black Sea by the Danube (and possibly by the Dniester, Bug and Dnieper) River that may further be dispersed southward by marine currents; (B) continental run-off from the closest landmasses (SE Bulgaria and NW Turkey); (C) wind-blown loess particles from the Danube Plain, Carpathian Mountains and Ukraine; (D) wind-blown dust from the Sahara Desert; (E) volcanic ash from Quaternary eruptions around the Black Sea. Two main scenarios may be considered for explaining the isotopic composition of the studied sediments: either there was a supply from a single source that has a somewhat heterogeneous isotopic character that fits the minor isotopic variations among the sediments deposited at different times and sites; or mixing occurred between two, or more, isotopically different components supplied from different provenances. This implies a thorough mixing of the components that must be delivered at quite constant proportions over time. Uniform isotope compositions can also be reached if one of the components is either much more abundant, or it has much higher element (Sr, Nd and Pb) concentrations compared to the other components, or both. From an isotopic point of view, it appears that the observed combination of radiogenic Sr ($^{87}Sr/^{86}Sr \sim 0.719-0.722$), intermediate Nd ($\varepsilon Nd(0) \sim -8$ to -10), and fairly evolved Pb ($^{206}Pb/^{204}Pb \sim 18.8-19.1$) is difficult to reconcile with a known, single source, and the presence of both felsic and more mafic crustal components seems logical. Nardone and Faure (1978) analyzed the detrital fraction of sediments from the central Black Sea and suggested that their variable Sr isotope composition being clearly different from our Black Sea data could be explained by a binary mixing of a felsic (originating from areas north of the Black Sea) and a mafic (from areas south of the Black Sea) rock component. It
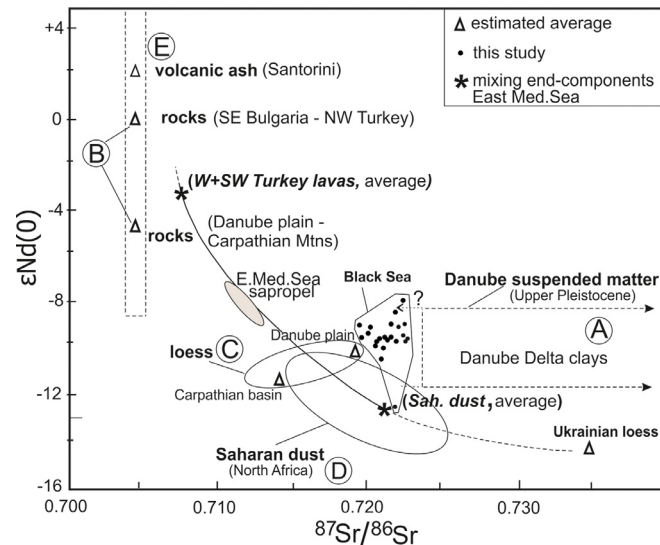
Figure 7   Correlation between $^{87}Sr/^{86}Sr$ versus $\varepsilon Nd(0)$ of the alumino-silicate component of the western Black Sea sediments. Sr-Nd-isotope composition of the rocks, clays, loess and dust from the possible provenances of this component are shown with letters. The solid hyperbolic curve, based on data from the Eastern Mediterranean Sea; the shaded area represents sapropels (Weldeab et al., 2002), refers to a binary mixing involving two end-components (W+SW Turkey lavas and Saharan dust) marked by stars. The uncertainties of the total isotopic range for potential source components with bearing on Black Sea data arise due to the limited amount of published data. Stippled boxes are likely to cover most of the isotopic variation for rocks (and clays) in the potential source areas. Encircled fields represent larger geographical regions and are designed to encompass average values of loess and dust sources. Data for the clays from the Danube Delta from Major et al. (2006); for the rocks from the SE Bulgaria and NW Turkey from Alici et al. (2002), Georgiev et al. (2009), Ruskov et al. (2006); for the rocks from the Danube plain and Carpathian mountains from Bojar et al. (2013), Dupont et al. (2002), Seghedi et al. (2007); for the ash from recent eruptions of the Santorini Volcano from Juul Petersen (2004); for the loess from the Danube plain and Carpathian basin from Schatz et al. (2015), Újvari et al. (2012); for the loess from Ukraine from Schatz et al. (2015); for the Saharan dust from North Africa from Grousset et al. (1998).

must be noted that their studied samples covered a much longer time span, including deposition during both glacial and inter-glacial periods, than what is the case in the present study. Weldeab et al. (2002) studied Late Pleistocene sapropels (S5 and S6 stages) and non-sapropels from the Eastern Mediterranean Sea. They argued that a binary mixing (cf. the hyperbolic mixing curve in Fig. 7) involving a Saharan dust component and a component representing Aegean basalts and/or Nile Delta sediments were consistent with the obtained Sr-Nd data. However, their sapropel data are distinctly different from our results from the Black Sea.

It remains speculative to assign realistic Sr (and Nd) isotope ratios to potential source components available during the appropriate time interval in the Black Sea. One feature illustrating this is that reported Sr-Nd isotope data from a geographical area may vary as a function of the material analyzed as shown by e.g., data from rocks, suspended matter and loess from the Danube plain (Fig. 7). Although quite limited, the variability in Sr-Nd isotope sapropel data indicates a mixing of different types of source components, and initially two riverine components (one from SE Bulgaria/NW Turkey and another one from the NW Black Sea) need to be considered. This is suggested for reasons of proximity (SE Bulgaria/NW Turkey) and because the rivers emptying in the NW Black Sea, in particular, the Danube River, are known to have supplied huge amounts of suspended material into the Black Sea that could further be carried southwards by

surface currents (Murray et al., 2007). Four clay fractions separated from the sediments of the Danube Delta (Major et al., 2006), covering the time span 19—11 ka BP, have variable radiogenic compositions with $^{87}Sr/^{86}Sr$ ranging between 0.723 and 0.751, whereas the other samples are much less radiogenic. These shifts to higher isotopic values may be related to short-lived inputs from a high $^{87}Sr/^{86}Sr$ source associated with anomalous run-off into the Black Sea (Major et al., 2006). Although there are no $^{87}Sr/^{86}Sr$ data available for the suspended matter in the NW Black Sea during the ~9 to 3 ka BP interval, it appears possible that a radiogenic component (schematically constrained to the box indicated by letter A in Fig. 7) was available at this time period. Its Nd isotope composition may be similar to data known for the Danube plain (Fig. 7). To the best of our knowledge, no corresponding Sr isotope data are available for the suspended matter entering the SW Black Sea (run-off from SE Bulgaria/NW Turkey). However, the isotope composition of the bedrock in this landmass (Alici et al., 2002; Georgiev et al., 2009; Ruskov et al., 2006) suggests that released riverine suspended matter is expected to have quite unradiogenic Sr and relatively radiogenic Nd values (cf. component B in Fig. 7). A NW (Black Sea) riverine suspended matter component could possibly also carry loess soils known to cover large parts of the Danube drainage basin and its surroundings. Its average Sr-Nd isotope composition (cf. component C in Fig. 7) is fairly similar to the published data from the Danube

plain, but extends to somewhat less radiogenic Sr isotope compositions. For the given assumptions, a mixing involving a predominant NW riverine component diluted with a SW riverine component can apparently produce data that are largely consistent with the Sr-Nd isotope composition of the studied sediments, which were deposited over a time span of ~6 ka. Besides, given that deposition of Saharan dust has been recognized in many areas of the northern hemisphere, including the Eastern Mediterranean (Papayannis et al., 2005), this type of source (component D in Fig. 7) must also be considered. Actually, the spread in Nd isotope ratios could indicate a mix between an aeolian (average) Saharan and a combined (NW+SW Black Sea) riverine component and, in particular, the unradiogenic Nd isotope value for the PLC-203 (260−262) sample (εNd(0) = −12.5) argues for a Saharan dust contribution. Moreover, one cannot reject the possibility of certain air-borne transportation of material from loess-covered landmasses north-west of the basin.

It may also be mentioned that tephra from the large Santorini eruption in ~3300 BP has been identified in Unit II of the Black Sea sediments (Guichard et al., 1993), but not in the other units sampled in the present study. However, the tephra occupies only a ca 1cm thick layer and the Sr-Nd isotope compositions of the Santorini volcanic products (Juul Petersen, 2004) and those of the hypothetical ash-fall related to the Quaternary volcanism in western Anatolia (Alici et al., 2002 and references therein) exhibit average values far from our data (cf. component E in Fig. 7). Therefore, in the light of the Sr-Nd isotope systematics being uniform for all the three stratigraphic units, we infer that the possible effect of any kind of ash-fall was insignificant.

Due to the lack of information about the prehistoric Pb isotopic composition of the riverine input to the Black Sea we cannot provide a detailed discussion about the sources of the Pb isotopes. Generally, the obtained Pb isotope compositions are relatively evolved and the similarity in data indicates a continuous supply from a crustal source that did not change significantly during the ongoing sedimentation. It is important to note that Pb in modern and even historical riverine input in the region likely will be influenced to a variable extent by anthropogenic Pb. In general, anthropogenic Pb addition to lake or marine sediments in the European region causes a shift in the Pb isotopes to lower ratios (e.g., Kamenov et al., 2009; Shotyk et al., 1998). Environmental archives show that the onset of Pb pollution in Europe began around 3000 years ago, with particular strong anthropogenic Pb input around 2000 years ago during the Roman Empire (Shotyk et al., 1998). Although we do not have exact dates for the analyzed sediment samples in Unit I, the boundary between Units I and II is dated to ~3000 BP (Kwiecien et al., 2008). Therefore, it is quite possible that the slight decrease in ^{206}Pb/^{204}Pb at the upper levels of Unit I (Fig. 5) can be a result of the incorporation of anthropogenic Pb in these sediments.

6. Conclusions

The last transition of the Black Sea from an oxic limnic to anoxic-euxinic marine basin at the beginning of the Holocene Epoch had a significant impact on the enrichment (or depletion) of a range of elements in the deep-sea sediments. At the onset of this transition, the deep waters evolved from oxic through suboxic to euxinic. Large amounts of Fe were remobilized through a benthic redox shuttle mechanism from the sediment when the suboxic conditions were established and prevailed over the abyssal plain and lower continental slope. With increasing euxinia in the deep pool, the mobilized Fe^{2+} was quantitatively removed to the sediment, which was recorded as Fe enrichment at the base of the lower Holocene Unit II. Sediment beneath the euxinic pool could not further release dissolved Fe and the only Fe^{2+} supply came from the narrow zone where the suboxic transition layer between the euxinic (deep) and oxic (surface) waters impinged the continental slope. The reduced Fe flux to the euxinic pool (recorded as weak Fe enrichment in the sedimentary archive) sharply increased when the rising suboxic layer impinged the continental shelf. The increased Fe supply was recorded as a second peak of the Fe enrichment at the top of Unit II. The vertical distribution of the Mn enrichment in the sediments seems to be principally controlled by the diagenetic dissolution of solid Mn phases in Unit II, Mn^{2+} upward diffusion to and re-precipitation in Unit I. Barium enrichment (depletion) in the studied sediments is controlled by diagenetic reactions: sulfate reduction and methanogenesis. Vertical Ba profile suggests that the sulfate-methane transition (important redox boundary for the Ba cycle) in the studied area is localized within the middle part of Unit II and the current authigenic $BaSO_4$ front is at the Unit II/Unit I boundary. The major part of Cu and Co, and partly Ni, Zn, Cr, W, Mo, V, Cd and Sb (in the upper Unit III and lower Unit II) are interpreted to have co-precipitated with Fe in the euxinic deep waters and been incorporated into authigenic Fe-sulfides. Nickel, Zn, Cr and W distributions in the upper Unit I are controlled by diagenetic processes. Vertical enrichment profiles of Mo, V, Cd and Sb are affected by basin reservoir effect. The U enrichment at the base of Unit II is inferred to be at the expense of the U inventory of the deepwater pool and a result of inorganic reduction of U at euxinic conditions. The U enrichment in Unit I is supposed to be a result of the bottom seawater U influx. The high field strength elements (Zr, Hf, Nb and Ta) are closely linked to the detrital component and their depletion in the organic-rich Units II and I reflects dilution of the detrital component with biogenic. The weak enrichments of REE, Sn and Th in all the three stratigraphic units are seemingly controlled by adsorption on clay minerals. Strontium depletion and enrichment are controlled by the decrease and increase of the biogenic $CaCO_3$ content.

According to the Sr-Nd-Pb-isotope studies, the alumino-silicate fraction (terrigenous component) of the studied sediments is best explained by a relatively stable influx of a dominant Danube plain component admixed with lesser amounts of material delivered as dust from the Sahara Desert and suspended matter from rivers draining the SE Bulgaria and NW Turkey.

Acknowledgments

References

Aagaard, P., 1974. Rare earth elements adsorption on clay minerals. Bull. Groupe Franç. Argiles 26 (2), 193—199.

Algeo, T.J., Lyons, T.W., 2006. Mo-total organic carbon covariation in modern anoxic marine environments: Implications for analysis of paleoredox and paleohydrographic conditions. Paleoceanography 21 (1). art. no. PA1016, 23 pp., https://doi.org/10.1029/2004PA001112 .

Alici, P., Temel, A., Gourgaud, A., 2002. Pb-Nd-Sr isotope and trace element geochemistry of Quarternary extension-related alkaline magmatism: a case study of Kula region (western Anatolia, Turkey). J. Volcanol. Geoth. Res. 115 (3—4), 487—510, https://doi.org/10.1016/S0377-0273(01)00328-6.

Aminot, A., Kérouel, R., 2007. Dosage automatique des nutriments dans les eaux marines: méthodes en flux continu. Ed. Ifremer, Méthodes d'analyse en milieu marin, 188 pp.

Anderson, T.F., Raiswell, R., 2004. Sources and mechanisms for the enrichment of highly reactive iron in euxinic Black Sea sediments. Am. J. Sci. 304 (3), 203—233, https://doi.org/10.2475/ajs.304.3.203.

Arkhangel'skii, A.D., Strakhov, N.M., 1938. Geologicheskoe stroenie i istoriya razvitiya Chernogo morya (Geological structure and history of the evolution of the Black Sea). Izv. Akad. Nauk S.S.S.R. 10, 3—104.

Bahr, A., Lamy, F., Arz, H.W., Kuhlmann, H., Wefer, G., 2005. Late glacial to Holocene climate and sedimentation history in the NW Black Sea. Mar. Geol. 214 (4), 309—322, https://doi.org/10.1016/j.margeo.2004.11.013.

Bahr, A., Lamy, F., Arz, H.W., Major, C., Kwiecien, O., Wefer, G., 2008. Abrupt changes of temperature and water chemistry in the late Pleistocene and early Holocene Black Sea. Geochem. Geophy. Geosy. 9 (1). art. no. Q01004, 16 pp., https://doi.org/10.1029/2007GC001683 .

Barnes, C.E., Cochran, J.K., 1991. Geochemistry of uranium in Black Sea sediments. Deep-Sea Res. 38, S1237—S1254.

Bayon, G., German, C.R., Boella, R.M., Milton, J.A., Taylor, R.N., Nesbitt, R.W., 2002. An improved method for extracting marine sediment fractions and its application to Sr and Nd isotopic analysis. Chem. Geol. 187 (3—4), 179—199, https://doi.org/10.1016/S0009-2541(01)00416-8.

Berner, R.A., 1981. Authigenic mineral formation resulting from organic matter decomposition in modern sediments. Fortschrit. Mineral. 59 (1), 117—135.

Bojar, A.-V., Dodd, J., Seghedi, I., 2013. Isotope geochemistry (O, H and Sr) of Late Cretaceous volcanic rocks, Haţeg basin, South Carpathians, Romania. J. Geol. Soc. London Spec. Publ. 382, 203—211, https://doi.org/10.1144/SP382.10.

Boulègue, J., Lord III, C.J., Church, T.M., 1982. Sulfur speciation and associated trace metals (Fe, Cu) in the porewaters of Great Marsh, Delaware. Geochim. Cosmochim. Acta 46 (3), 453—464, https://doi.org/10.1016/0016-7037(82)90236-8.

Bruque, S., Mozas, T., Rodriguez, A., 1980. Factors influencing retention of lanthanide ions by montmorillonite. Clay Miner. 15 (4), 413—420, https://doi.org/10.1180/claymin.1980.015.4.08.

Brzezinski, M.A., 1985. The Si:C:N ratio of marine diatoms: interspecific variability and the effect of some environmental variables. J. Phycol. 21 (3), 347—357, https://doi.org/10.1111/j.0022-3646.1985.00347.x.

Calvert, S.E. , 1990. Geochemistry and origin of the Holocene sapropel in the Black Sea. In: Ittekkot, V., Kempe, S., Michaelis, W., Spitzy, A. (Eds.), Facets of Modern Biogeochemistry. Springer-Verlag, Berlin, 326—352.

Calvert, S.E., Batchelor, C.H. , 1978. Major and minor element geochemistry of sediments from Hole 379A, Leg 42B, Deep Sea Drilling Project. In: Usher, J.L., Supko, P. (Eds.), Initial Reports of the Deep Sea Drilling Project. U.S. Government Printing Office, Washington, 527—541.

Calvert, S.E., Pedersen, T.F., 1993. Geochemistry of Recent oxic and anoxic marine sediments: Implications for the geological record. Mar. Geol. 113 (1—2), 67—88, https://doi.org/10.1111/10.1016/0025-3227(93)90150-T.

Calvert, S.E., Karlin, R.E., 1998. Organic carbon accumulation in the Holocene sapropel of the Black Sea. Geology 26 (2), 107—110, https://doi.org/10.1130/0091-7613(1998)026⟨0107:OCAITH⟩2.3.CO;2.

Calvert, S.E., Vogel, J.S., Southon, J.R., 1987. Carbon accumulation rates and the origin of the Holocene sapropel in the Black Sea. Geology 15 (10), 918—921, https://doi.org/10.1130/0091-7613(1987)15⟨918:CARATO⟩2.0.CO;2.

Canfield, D.E., Lyons, T.W., Raiswell, R., 1996. A model for iron deposition to euxinic Black Sea sediments. Am. J. Sci. 296 (7), 818—834, https://doi.org/10.2475/ajs.296.7.818.

De Ignacio, C., Muñoz, M., Sagredo, J., Fernández-Santín, S., Johansson, Å, 2006. Isotope geochemistry and FOZO mantle component of the alkaline-carbonatitic association of Fuerteventura, Canary Islands, Spain. Chem. Geol. 232 (3—4), 99—113, https://doi.org/10.1016/j.chemgeo.2006.02.009.

Degens, E.T., Ross, D.A., 1972. Chronology of the Black Sea over the last 25,000 years. Chem. Geol. 10 (1), 1—16, https://doi.org/10.1016/0009-2541(72)90073-3.

Degens, E.T., Ross, D.A., 1974. The Black Sea — Geology, chemistry, and biology. In: Degens, E.T., Ross, D.A. (Eds.), American Assoc. Petroleum Geolog. Mem. 20. Tulsa, OK, 633 pp.

Degens, E.T., Khoo, F., Michaelis, W., 1977. Uranium anomaly in Black Sea sediments. Nature 269 (5629), 566—569, https://doi.org/10.1038/269566a0.

DeMaster, D.J., 1981. The supply and accumulation of silica in the marine environment. Geochim. Cosmochim. Acta 45 (10), 1715—1732, https://doi.org/10.1016/0016-7037(81)90006-5.

DeMaster, D.J., Nelson, T.M., Harden, S.L., Nittrouer, C.A., 1991. The cycling and accumulation of biogenic silica and organic carbon in Antarctic deep-sea and continental margin environments. Mar. Chem. 35 (1—4), 489—502, https://doi.org/10.1016/S0304-4203(09)90039-1.

Dupont, A., Auwera, J.V., Pin, C., Marincea, S., Berza, T., 2002. Trace element and isotope (Sr, Nd) geochemistry of porphyry- and skarn mineralising Late Cretaceous intrusions from Banat, western South Carpathians. Romania. Miner. Deposita 37 (6—7), 568—586, https://doi.org/10.1007/s00126-002-0274-7.

Eckert, S., Brumsack, H.-J., Severmann, S., Schnetger, B., März, C., Fröllje, H., 2013. Establishment of euxinic conditions in the Holocene Black Sea. Geology 41 (4), 431—434, https://doi.org/10.1130/G33826.1.

Emerson, S., Hedges, J. , 2003. Sediment diagenesis and benthic flux. In: Elderfield, H. (Ed.), The Oceans and Marine Geochemistry. Treatise on Geochemistry, 1st edn.. Elsevier, Amsterdam, 293—319.

Franke, C., Robin, E., Henkel, S., Kasten, S., Bleil, U., 2009. Iron sulfide minerals in Black Sea sediments. In: EGU General Assembly 2009, Vienna 19—24.04.2009, 10672.

Garbe-Schönberg, C.-D., 1993. Simultaneous determination of thirty-seven trace elements in twenty-eight international rock standards by ICP-MS. Geostandard Newslett 17 (1), 81—97, https://doi.org/10.1111/j.1751-908X.1993.tb00122.x.

Georgiev, S., Marchev, P., Heinrich, C.A., Von Quadt, A., Peytcheva, I., Manetti, P., 2009. Origin of nepheline-normative high-K ankaramites and the evolution of Eastern Srednogorie Arc in SE Europe. J. Petrol. 50 (10), 1899—1933, https://doi.org/10.1093/petrology/egp056.

German, C.R., Holliday, B.P., Elderfield, H., 1991. Redox cycling of rare earth elements in the suboxic zone of the Black Sea. Geochim. Cosmochim. Acta 55 (12), 3553—3558, https://doi.org/10.1016/0016-7037(91)90055-A.

Glenn, C.R., Arthur, M.A., 1985. Sedimentary and geochemical indicators of productivity and oxygen contents in modern and ancient basins: The Holocene Black Sea as the "type" anoxic basin. Chem. Geol. 48 (1—4), 325—354, https://doi.org/10.1016/0009-2541(85)90057-9.

Goldberg, E.D., 1954. Marine geochemistry 1. Chemical scavengers of the sea. J. Geol. 62 (3), 249—265, https://www.jstor.org/stable/30080120.

Goldberg, E.D., 1961. Chemical and mineralogical aspects of deep-sea sediments. Phys. Chem. Earth 4, 281—302, https://doi.org/10.1016/0079-1946(61)90009-X.

Goldberg, E.D., Arrhenius, G.O.S., 1958. Chemistry of Pacific pelagic sediments. Geochim. Cosmochim. Acta 13 (2—3), 153—212, https://doi.org/10.1016/0016-7037(58)90046-2.

Goldschmidt, V.M., 1954. Geochemistry. The Clarendon Press, Oxford, 730 pp.

Grousset, F.E., Parra, M., Bory, A., Martinez, P., Bertrand, P., Shimmield, G., Ellam, R.M., 1998. Saharan wind regimes traced by the Sr-Nd isotopic composition of the subtropical Atlantic sediments: last glacial maximum vs. today. Quat. Sci. Rev. 17 (4—5), 395—409, https://doi.org/10.1016/S0277-3791(97)00048-6.

Guichard, F., Carey, S., Arthur, M.A., Sigurdsson, H., Arnold, M., 1993. Tephra from the Minoan eruption of Santorini in sediments of the Black Sea. Nature 363 (6430), 610—612, https://doi.org/10.1038/363610a0.

Haley, B.A., Frank, M., Spielhagen, R.F., Fietzke, J., 2008. Radiogenic isotope record of Arctic Ocean circulation and weathering inputs of the past 15 million years. Paleoceanography 23 (1). art. no. PA1S13, 16 pp., https://doi.org/10.1029/2007PA001486 .

Hay, B.J., Honjo, S., Kempe, S., Ittekkot, V.A., Degens, E.T., Konuk, T., Izdar, E., 1990. Interannual variability in particle flux in the southwestern Black Sea. Deep Sea Res. 37 (6), 911—928, https://doi.org/10.1016/0198-0149(90)90103-3.

Hedge, C.E., Walthall, F.G., 1963. Radiogenic strontium-87 as an index to geologic processes. Science 140 (3572), 1214—1217, https://doi.org/10.1126/science.140.3572.1214-a.

Henkel, S., Mogollón, J.M., Nöthen, K., Franke, C., Bogus, K., Robin, E., Bahr, A., Blumenberg, M., Pape, T., Seifert, R., März, C., de Lange, G.J., Kasten, S., 2012. Diagenetic barium cycling in Black Sea sediments — A case study for anoxic marine environments. Geochim. Cosmochim. Acta 88, 88—105, https://doi.org/10.1016/j.gca.2012.04.021.

Hirst, D.M., 1974. Geochemistry of sediments from eleven Black Sea cores. In: Degens, E.T., Ross, D.A. (Eds.), The Black Sea — Geology, Chemistry, and Biology. American Assoc. Petroleum Geolog. Mem. 20, Tulsa, OK, 430—455.

Hsü, K.J. , 1978. Correlation of Black Sea sequences. In: Usher, J.L., Supko, P. (Eds.). Initial Reports of the Deep Sea Drilling Project. Vol. 42, pt. 2. U.S. Gov. Printing Office, Washington, 489—497.

Huerta-Diaz, M.A., Morse, J.W., 1992. Pyritization of trace metals in anoxic marine sediments. Geochim. Cosmochim. Acta 56 (7), 2681—2702, https://doi.org/10.1016/0016-7037(92)90353-K.

Hurtgen, M.T., Lyons, T.W., Ingall, E.D., Cruse, A.M., 1999. Anomalous enrichments of iron monosulfide in euxinic marine sediments and the role of H_2S in iron sulfide transformations: Examples from Effingham Inlet, Orca Basin, and the Black Sea. Am. J. Sci. 299 (7), 556—588, https://doi.org/10.2475/ajs.299.7-9.556.

Jochum, K.P., Nohl, U., Herwig, K., Lammel, E., Stoll, B., Hofmann, A.W., 2005. GeoReM: A new geochemical database for reference materials and isotopic standards. Geostand. Geoanal. Res. 29 (3), 333—338, https://doi.org/10.1111/j.1751-908X.2005.tb00904.x.

Juul Petersen, A.D., 2004. A geological and petrological study of dikes in the Megalo Vouno volcano complex, Santorini. Department of Geology, Copenhagen Univ., 142 pp.

Kamenov, G.D., Dekov, V.M., Willingham, A.L., Savelli, C., Belucci, L.G., 2009. Anthropogenic Pb in recent hydrothermal sediments from the Tyrrhenian Sea: Implications for seawater Pb control on low-temperature hydrothermal systems. Geology 37 (2), 111—114, https://doi.org/10.1130/G25104A.1.

Koning, E., Epping, E., Van Raaphorst, W., 2002. Determining biogenic silica in marine samples by tracking silicate and aluminium concentrations in alkaline leaching solutions. Aquat. Geochem. 8 (1), 37—67, https://doi.org/10.1023/A:1020318610178.

Konovalov, S.K., Luther III, G.W., Yücel, M., 2007. Porewater redox species and processes in the Black Sea sediments. Chem. Geol. 245 (3—4), 254—274, https://doi.org/10.1016/j.chemgeo.2007.08.010.

Kwiecien, O., Arz, H.W., Lamy, F., Wulf, S., Bahr, A., Röhl, U., Haug, G.H., 2008. Estimated reservoir ages of the Black Sea since the Last Glacial. Radiocarbon 50 (1), 99—118, https://doi.org/10.1017/S0033822200043393.

Little, S.H., Vance, D., Lyons, T.W., McManus, J., 2015. Controls on trace metal authigenic enrichment in reducing sediments: Insights from modern oxygen-deficient settings. Am. J. Sci. 315 (2), 77—119, https://doi.org/10.2475/02.2015.01.

Lyons, T.W., Severmann, S., 2006. A critical look at iron paleoredox proxies: New insights from modern euxinic marine basins. Geochim. Cosmochim. Acta 70 (23), 5698—5722, https://doi.org/10.1016/j.gca.2006.08.021.

Major, C., Ryan, W., Lericolais, G., Hajdas, I., 2002. Constraints on Black Sea outflow to the Sea of Marmara during the last glacial-interglacial transition. Mar. Geol. 190 (1—2), 19—34, https://doi.org/10.1016/S0025-3227(02)00340-7.

Major, C.O., Goldstein, S.L., Ryan, W.B.F., Lericolais, G., Piotrowski, A.M., Hajdas, I., 2006. The co-evolution of Black Sea level and composition through the last deglaciation and its paleoclimatic significance. Quat. Sci. Rev. 25 (17—18), 2031—2047, https://doi.org/10.1016/j.quascirev.2006.01.032.

McLennan, S.M. , 1989. Rare earth elements in sedimentary rocks: Influence of provenance and sedimentary processes. In: Lipin, B.R., McKay, G.A. (Eds.). Geochemistry and Mineralogy of Rare Earth Elements. Reviews in Mineralogy, 21, 169—200.

McManus, J., Berelson, W.M., Klinkhammer, G.P., Kilgore, T.E., Hammond, D.E., 1994. Remobilization of barium in continental margin sediments. Geochim. Cosmochim. Acta 58 (22), 4899—4907, https://doi.org/10.1016/0016-7037(94)90220-8.

McManus, J., Berelson, W.M., Klinkhammer, G.P., Johnson, K.S., Coale, K.H., Anderson, R.F., Kumar, N., Burdige, D.J., Hammond, D.E., Brumsack, H.J., McCorkle, D.C., Rushdi, A., 1998. Geochemistry of barium in marine sediments: Implications for its use as a paleoproxy. Geochim. Cosmochim. Acta 62 (21—22), 3453—3473, https://doi.org/10.1016/S0016-7037(98)00248-8.

Monnin, C., Wheat, C.G., Dupre, B., Elderfield, H., Mottl, M.M., 2001. Barium geochemistry in sediment pore waters and formation waters of the oceanic crust on the eastern flank of the Juan de Fuca Ridge (ODP Leg 168). Geochem. Geophy. Geosy. 2. (1), art. no. 2000GC000073, 15 pp., https://doi.org/10.1029/2000GC000073 .

Morford, J.L., Emerson, S., 1999. The geochemistry of redox sensitive trace metals in sediments. Geochim. Cosmochim. Acta 63 (11—12), 1735—1750, https://doi.org/10.1016/S0016-7037(99)00126-X.

Murray, J.W., Jannasch, H.W., Honjo, S., Anderson, R.F., Reeburgh, W.S., Top, Z., Friederich, G.E., Codispoti, L.A., Izdar, E., 1989. Unexpected changes in the oxic/anoxic interface in the Black Sea. Nature 338 (6214), 411—413, https://doi.org/10.1038/338411a0.

Murray, J.W., Top, Z., Özsoy, E., 1991. Hydrographic properties and ventilation of the Black Sea. Deep-Sea Res. 38 (S2), S663—S689, https://doi.org/10.1016/S0198-0149(10)80003-2.

Murray, J.W., Stewart, K., Kassakian, S., Krynytzky, M., DiJulio, D. , 2007. Oxic, suboxic, and anoxic conditions in the Black Sea. In: Yanko-Hombach, V., Gilbert, A.S., Panin, N., Dolukhanov, P.M. (Eds.), The Black Sea Flood Question: Changes in Coastline, Climate, and Human Settlement. Springer, Dordrecht, 1—21.

Nardone, C.D., Faure, G., 1978. A study of sedimentation at DSDP Hole 379A, Black Sea, based on the isotopic composition of strontium. In: Usher, J.L., Supko, P. (Eds.), Initial Reports of the Deep Sea Drilling Project. Vol. 42, pt. 2. U.S. Government Printing Office, Washington, 607-615.

Neveskii, E.N., 1967. Protsessy osadkoobrazovaniya v pribrezhnoy zone morya (Processes of sediment formation in the near-shore zone of the sea). Nauka, Moscow, 255 pp.

Papayannis, A., Balis, D., Amiridis, V., Chourdakis, G., Tsaknakis, G., Zerefos, C., Castanho, D.A., Nickovic, S., Kazadzis, S., Grabowski, J., 2005. Measurements of Saharan dust aerosols over the Eastern Mediterranean using elastic backscatter — Raman lidar, spectrophotometric and satellite observations in the frame of the EARLINET project. Atmos. Chem. Phys. 5 (8), 2065—2079, https://doi.org/10.5194/acpd-5-2075-2005.

Pettijohn, F.J., Potter, P.E., Siever, R., 1972. Sand and Sandstone. Springer, New York, 618 pp.

Pilskaln, C.H., Pike, J., 2001. Formation of Holocene sedimentary laminae in the Black Sea and the role of the benthic flocculent layer. Paleoceanography 16 (1), 1—19, https://doi.org/10.1029/1999PA000469.

Pin, C., Zalduegui, J.F.S., 1997. Sequential separation of light rare-earth elements, thorium and uranium by miniaturized extraction chromatography: Application to isotopic analyses of silicate rocks. Anal. Chim. Acta 339 (1—2), 79—89, https://doi.org/10.1029/1999PA000469.

Plank, T., Langmuir, C.H., 1998. The chemical composition of subducting sediment and its consequences for the crust and mantle. Chem. Geol. 145 (3—4), 325—394, https://doi.org/10.1016/S0009-2541(97)00150-2.

Ragueneau, O., Dittert, N., Pondaven, P., Tréguer, P., Corrin, L., 2002. Si/C decoupling in the world ocean: is the Southern Ocean different? Deep-Sea Res. Pt. II 49 (16), 3127—3154, https://doi.org/10.1016/S0967-0645(02)00075-9.

Ragueneau, O., Regaudie-de-Gioux, A., Moriceau, B., Gallinari, M., Vangriesheim, A., Baurand, F., Khripounoff, A., 2009. A benthic Si mass balance on the Congo margin: Origin of the 4000 m DSi anomaly and implications for the transfer of Si from land to ocean. Deep-Sea Res. Pt. II 56 (23), 2197—2207, https://doi.org/10.1016/j.dsr2.2009.04.003.

Raiswell, R., Anderson, T.F., 2005. Reactive iron enrichment in sediments deposited beneath euxinic bottom waters: constraints on supply by shelf recycling. Geol. Soc. London, Spec. Publ. 248 (1), 179—194, https://doi.org/10.1144/GSL.SP.2005.248.01.10.

Ross, D.A. , 1978. Black Sea stratigraphy. In: Usher, J.L., Supko, P. (Eds.). Initial Reports of the Deep Sea Drilling Project. Vol. 42, pt. 2. U.S. Gov. Printing Office, Washington, 17—26.

Ross, D.A., Degens, E.T. , 1974. Recent sediments of the Black Sea. In: Degens, E.T., Ross, D.A. (Eds.). The Black Sea — Geology, Chemistry, and Biology. Vol. 20. American Association of Petroleum Geologists Memoir, Tulsa, Oklahoma, 183—199.

Ross, D.A., Degens, E.T., MacIlvaine, J., 1970. Black Sea: Recent sedimentary history. Science 170 (3954), 163—165, https://doi.org/10.1126/science.170.3954.163.

Ross, D.A., Stoffers, P., Trimonis, E.S. , 1978. Black Sea sedimentary framework. In: Usher, J.L., Supko, P. (Eds.). Initial Reports of the Deep Sea Drilling Project. Vol. 42, pt. 2. U.S. Gov. Printing Office, Washington, 359—372.

Rudnick, R.L., Gao, S. , 2003. Composition of the continental crust. In: Rudnick, R.L. (Ed.). The Crust. Treatise on Geochemistry, Vol. 3, 1st edn.. Elsevier, Amsterdam, 1—64.

Ruskov, K., von Quadt, A., Peytcheva, I., Georgiev, S., Strashimirov, S., 2006. Geochemical and Sr-Nd isotope constraints on the Late Cretaceous magmatism in the area of the Zidarovo ore field. In: Annual of the University of mining and geology "St. Ivan Rilski", Vol. 49, Pt. I, Geology and Geophysiscs, 1—6.

Schatz, A.-K., Qi, Y., Siebel, W., Wu, J., Zöller, L., 2015. Tracking potential source areas of Central European loess; examples from Tokaj (HU), Nussloch (D) and Grub (AT). Open Geosci. 7 (1), 678—720, https://doi.org/10.1515/geo-2015-0048.

Seghedi, I., Bojar, A.-V., Downes, H., Roşu, E., Tonarini, S., Mason, P., 2007. Generation of normal and adakite-like calc-alkaline magmas in a non-subductional environment: An Sr-O-H isotopic study of the Apuseni Mountains neogene magmatic province, Romania. Chem. Geol. 245 (1—2), 70—88, https://doi.org/10.1016/j.chemgeo.2007.07.027.

Shotyk, W., Weiss, D., Appleby, P.G., Cheburkin, A.K., Frei, R., Gloor, M., Kramers, J.D., Reese, S., Van Der Knaap, W.O., 1998. History of atmospheric lead deposition since 12,370 ^{14}C yr BP from a peat bog, Jura Mountains, Switzerland. Science 281 (5383), 1635—1640, https://doi.org/10.1126/science.281.5383.1635.

Soulet, G., Ménot, G., Lericolais, G., Bard, E., 2011. A revised calendar age for the last reconnection of the Black Sea to the global ocean. Quat. Sci. Rev. 30 (9—10), 1019—1026, https://doi.org/10.1016/j.quascirev.2011.03.001.

Stoffers, P., Müller, G. , 1978. Mineralogy and lithofacies of Black Sea sediments Leg 42B Deep Sea Drilling Project. In: Usher, J.L., Supko, P. (Eds.), Initial Reports of the Deep Sea Drilling Project. U.S. Government Printing Office, Washington, 373—411.

Stoffers, P., Degens, E.T., Trimonis, E.S. , 1978. Stratigraphy and suggested ages of Black Sea sediments cored during Leg 42B. In: Usher, J.L., Supko, P. (Eds.), Initial Reports of the Deep Sea Drilling Project. U.S. Government Printing Office, Washington, 483—487.

Takahashi, Y., Tada, A., Shimizu, H., 2004. Distribution pattern of rare earth ions between water and montmorillonite and its relation to the sorbed species of the ions. Anal. Sci. 20 (9), 1301—1306, https://doi.org/10.2116/analsci.20.1301.

Tertre, E., Berger, G., Castet, S., Loubet, M., Giffaut, E., 2005. Experimental sorption of Ni^{2+}, Cs^+ and Ln^{3+} onto a montmorillonite up to 150°C. Geochim. Cosmochim. Acta 69 (21), 4937—4948, https://doi.org/10.1016/j.gca.2005.04.024.

Todt, W., Cliff, R.A., Hanser, A., Hofmann, A.W. , 1996. Evaluation of a [202]Pb-[205]Pb double spike for high-precision lead isotopic analysis. In: Basu, A., Hart, S.R. (Eds.), Earth Processes: Reading the Isotopic Code. Geophys. Monogr. Ser. Vol. 95. American Geophys. Union, 429—437.

Újvári, G., Varga, A., Ramos, F.C., Kovács, J., Németh, T., Stevens, T., 2012. Evaluating the use of clay mineralogy, Sr-Nd isotopes and zircon U-Pb ages in tracking dust provenance: An example from loess of the Carpathian Basin. Chem. Geol. 304—305, 83—96, https://doi.org/10.1016/j.chemgeo.2012.02.007.

Vance, D., Burton, K., 1999. Neodymium isotopes in planktonic foraminifera: a record of the response of continental weathering and ocean circulation rates to climate change. Earth Planet. Sci. Lett. 173 (4), 365—379, https://doi.org/10.1016/S0012-821X(99)00244-7.

Wan, Y.X., Liu, C.Q., 2005. Study on adsorption of rare earth elements by kaolinite. J. Rare Earths 23 (3), 377—381.

Weldeab, S., Emeis, K.-C., Hemleben, C., Vennemann, T.W., Schulz, H., 2002. Sr and Nd isotope composition of Late Pleistocene sapropels and nonsapropelic sediments from the Eastern Mediterranean Sea: Implications for detrital influx and climatic conditions in the source areas. Geochim. Cosmochim. Acta 66 (20), 3585—3598, https://doi.org/10.1016/S0016-7037(02)00954-7.